Chapter 5

Radio Wave Propagation Phenomena from GPS Occultation Data Analysis

Alexey Pavelyev, Alexander Pavelyev, Stanislav Matyugov,
Oleg Yakovlev, Yuei-An Liou, Kefei Zhang and Jens Wickert

Additional information is available at the end of the chapter

http://dx.doi.org/10.5772/55480

1. Introduction

The aim of this book chapter is to reconsider the fundamental principle of radio-occultation (RO) remote sensing and to find new applications of RO method.

The RO remote sensing can be performed with any two cooperating satellites located on opposite sides with respect to the Earth's limb and moving to radio shadow. Several RO missions are working now aboard the Low Earth Orbit satellites. These missions provide global monitoring of the atmosphere and ionosphere of the Earth at different altitudes with high spatial resolution and accuracy. Their data are very important for meteorology, weather prediction. The RO data can be used to detect the climate changes, connections between the ionospheric, atmospheric processes, and solar activity, and to estimate conditions for radio navigation and radio location.

Up to now the RO inverse problem solution was based on the assumptions that the atmosphere and ionosphere are spherically symmetric and that the influence of turbulent and irregular structures on the retrieved vertical profiles of refractive index is insignificant [1,2]. The vertical profiles of refractive index are usually determined by measurement of the Doppler shift of radio wave frequency [1–3]. Information contained in the amplitude part of the radio-holograms was almost not addressed earlier, and this fact impeded separation of the contributions from layers and turbulent (small-scale) structures.

A new important relationship between the second-order time derivative (acceleration) of the phase path (eikonal), Doppler frequency, and intensity variations of the radio occultation (RO) signal was revealed by theoretical considerations and experimental analysis of the radio-holograms recorded onboard of the CHAMP and FORMOSAT-3 satellites [4–6]. Using the detected relationship, a possibility of determining the altitude, position, and inclination

of plasma layers in the ionosphere from the RO data has been revealed [4–8]. The proposed calculation technique is simpler than the phase-screen [9] and back-propagation methods [10, 11]. The detected relationship is also important for estimation of the total attenuation of radio waves in a satellite communication link by combining the analysis of information contained in the amplitude and phase channels of the radio-holograms. The mentioned relationship makes it possible to convert the eikonal acceleration (or the time derivative of the Doppler frequency shift) into the refractive attenuation.

The total absorption of radio waves in the decimeter wavelength range at a frequency of 930 MHz was earlier determined experimentally [12, 13] in the "MIR" orbital station–geostationary satellites communication link. In those papers, attenuation was removed from the amplitude data with the use of the time dependence of the derivatives of the phase and Doppler frequency shifts. Measurements of the total absorption for determining the water content in the stratosphere and troposphere will be performed in the future radio-occultation missions [14] at three frequencies near the water-vapor absorption line at the wavelength of 1.35 cm. For analysis and processing of these measurement data, a technique [15, 16] using the integral Fourier operators (Canonical Transform (CT) and Full Spectrum Inversion Fourier analysis (FSI)) is proposed. In [16, 17] a radio-holographic technique of the total absorption measurements has been previously proposed. Following this technique, the refractive attenuation effect on the amplitude of the field transformed by an integral Fourier operator is ruled out by using the relationship between the refractive attenuation and the second-order time derivative of the phase difference of the recorded and reference signals.

Unlike the methods used in [15–17], the eikonal acceleration/intensity technique does not use any integral transform and can be directly employed for determining the total absorption of radio waves in the case of significant refractive attenuation under the condition of single path propagation. Moreover, the combined analysis of the eikonal acceleration and radio wave intensity makes radio vision of the atmospheric and ionospheric layers possible, i.e., allows the layers to be detected by observing correlated variations in the eikonal acceleration and intensity against the background of an uncorrelated contribution of turbulent inhomogeneities and small-scale structures and permits one to measure the layer parameters.

The book chapter is organized as follows. In section 2 the basic rules are given for describing radio waves propagation in a spherically symmetric medium including a new relationship for the refractive attenuation. In section 3 an advanced eikonal /intensity technique is introduced and applied to find the total absorption from analysis of the RO data. In section 4 a locality principle and its applications to determining the location, slope, and height of plasma layers in the ionosphere are described. Comparison with the back-propagation radio-holographic method is carried out. In section 5 the seasonal changes of the bending angle during four years of observations in Moscow and Kamchatka areas are described. Conclusions and references are given in section 6 and section 7, respectively.

2. Basic rules for radio waves propagation in a spherically symmetric medium

To obtain basic relationships describing the radio wave propagation in a spherically symmetric medium it is necessary to use a formula [18] for electromagnetic field $\mathbf{E}$ in an inhomogeneous medium that follows from Maxwell equations:

$$\nabla^2\mathbf{E} + k_0^2 n^2 \mathbf{E} = -\text{grad}\left(\frac{\mathbf{E}\ \text{grad}\ \varepsilon}{\varepsilon}\right) \tag{1}$$

where k_0 is the wave number of radio wave in free space, n, ε are the refractive index and dielectric permittivity of medium, respectively. If vector $\mathbf{E}$ is perpendicular to grad ε, then (1) can be transformed to a homogeneous wave equation:

$$\nabla^2 E + k_0^2 n^2 E = 0 \tag{2}$$

where $E(\mathbf{r})$ is a component of the field $\mathbf{E}$. Solution of the eqn. (2) can be presented in the form [18,19]:

$$E(\mathbf{r}) = E_a(\mathbf{r})\ \exp\left(ik_0\psi(r)\right) \tag{3}$$

where $E_a(\mathbf{r})$, $\psi(r)$ – are the complex amplitude and phase path (eikonal) of radio wave. The eikonal $\psi(r)$ can be described by relationship:

$$\psi(r) = \int n(\mathbf{r})\ dl \tag{4}$$

where λ_0 is the wavelength in free space, and integration in (4) is fulfilled along a ray trajectory of radio wave. After substitution (3) into (2) one can obtain:

$$\nabla^2 E + k_0^2 n^2 E = \left\{\begin{matrix}\nabla^2 E_a(\mathbf{r}) - \kappa_0^2 E_a(\mathbf{r})(\nabla\psi)^2 + k_0^2 n^2 E_a(\mathbf{r}) \\ +i\kappa_0\left[2(\nabla E_a(\mathbf{r})\nabla\psi) + E_a(\mathbf{r})\nabla^2\psi\right]\end{matrix}\right\}\exp\left(ik_0\psi\right) = 0 \tag{5}$$

Two terms in the curly brackets of equation (5) formally differ by a factor – the imaginary unit i. Therefore to fulfill equation (5) these terms must be zero separately [18]:

$$\nabla^2 E_a(\mathbf{r}) - \kappa_0^2 E_a(\mathbf{r})\left(\nabla\ \psi\right)^2 + n^2(\mathbf{r})\kappa_0^2 E_a(\mathbf{r}) = 0 \tag{6}$$

$$2\nabla E_a(\mathbf{r})\nabla\ \psi + \ E_a(\mathbf{r})\nabla^2\psi\ = 0 \tag{7}$$

Under the geometric optics assumptions [18,19]:

$$\frac{\left|\nabla^2 E_a(\mathbf{r})\right|}{\left|\kappa_0^2\ E_a(\mathbf{r})\right|}\ << \left(\nabla\psi\right)^2,\ n^2(\mathbf{r}) \tag{8}$$

the next equations are valid [18,19]:

$$(\nabla\psi)^2 = n^2(\mathbf{r}); \quad |\nabla\psi| = n(\mathbf{r}); \nabla\psi = \mathbf{l_0} n(\mathbf{r}) \tag{9}$$

$$E_a(\mathbf{r})\nabla^2\psi + 2(\nabla E_a(\mathbf{r})\nabla\psi) = 0 \tag{10}$$

where $\mathbf{l}_0$ is a unit vector oriented along the radio ray. The first and second relationships (9) are the eikonal equations. Formula (10) connects variations of the eikonal ψ and gradient of amplitude $E_a(\mathbf{r})$. Relationship (10) is known as a transfer equation for the field amplitude [19].

It follows from the relationships (9) that the ray equation has a form [18,19]:

$$\frac{\partial}{\partial l}(\mathbf{l}_0 n) = \text{grad } n \tag{11}$$

where ∂l is an element of the length of the radio ray. In the case of spherical symmetry with a center located at the center of the Earth the gradient of the refractivity grad n and vector $\mathbf{r}$ have the same directions, and the impact parameter p is constant along the radio ray [18, 19]:

$$rn(r)\sin\gamma = p = \text{const} \tag{12}$$

where γ is the angle between directions to the center of spherical symmetry and tangent to the radio ray.

One can obtain a relationship for the refractive attenuation of radio wave by multiplying equation (10) by $E_a(\mathbf{r})$:

$$E_a^2(\mathbf{r})\nabla^2\psi + 2E_a(\mathbf{r})\left(\nabla E_a(\mathbf{r})\nabla\psi\right) = 0 \tag{13}$$

It follows from (13)

$$\text{div}\left(E_a^2(\mathbf{r})n(\mathbf{r})\,\mathbf{l}_0\right) = 0 \tag{14}$$

According to the Gauss theorem the next relationship is valid along a ray tube:

$$n(\mathbf{r})E_a^2(\mathbf{r})\Delta A = const \tag{15}$$

where ΔA is the cross section square of a ray tube.

The relationships (11), (12), and (15) present basic rules describing the ray direction and power conservation laws in the spherically symmetric medium. From (15) one can obtain important formula for the refractive attenuation when the transmitter and receiver are located in a medium with arbitrary values of the refraction index.

In the case of spherical symmetric medium one can consider according to [18,20] a ray tube having at point G in the plane of Figure 1 the angular size $d\gamma$. This tube in the figure plane

is bounded by lines GL and GL_1 (dotted line in Figure 1). The circle of radius R, with center at point O, intersects with the dotted line GL_1 at L_1, so that the arc $LL_1 = Rd\theta$. From the geometry (Figure 1) it follows that vector $\mathbf{LL}_2$ whose magnitude is $LL_2 = Rd\theta\cos\gamma_1$ perpendicular to the line GL_1. The side walls of the ray tube are located in the planes which are intersecting with straight line OG. The dihedral angle between these planes is equal to $d\gamma$. The size of the ray tube in the plane perpendicular to the figure plane at point L_1 is equal to $R\sin\theta d\gamma$. Therefore the cross section of the ray tube may be described by the relationship:

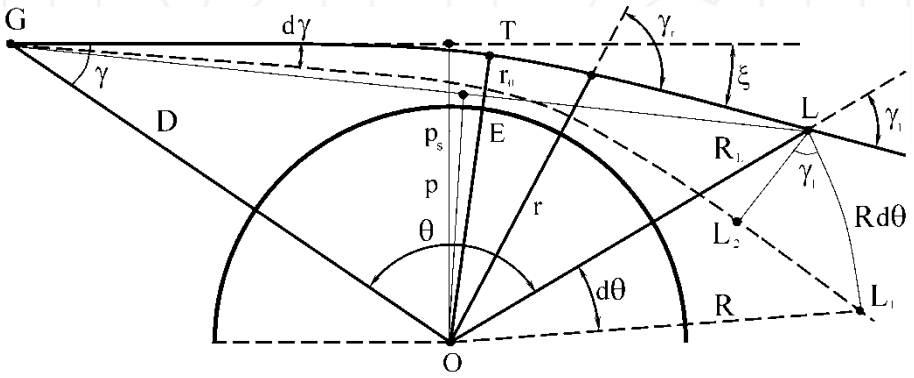

Figure 1. Ray tube in the radio occultation scheme. The center of spherical symmetry coincides with Earth's center O.

$$\Delta A = R^2\left(d\gamma\right)^2\frac{d\theta}{dp}\frac{dp}{d\gamma}\cos\gamma_1\sin\theta \tag{16}$$

where $R = R_L$ is the distance from point L_1 to the center of spherical symmetry, γ_1, θ are the angles between the direction to the center of spherical symmetry, tangent to the radio ray, and the direction to the transmitter of radio wave, respectively. $d\gamma$ is the angular size of the ray tube. The value $\frac{dp}{d\gamma}$ can be obtained from (12):

$$\frac{dp}{d\gamma} = n(D)D\cos\gamma = \sqrt{n^2(D)D^2 - p^2} \tag{17}$$

where D is the distance from transmitter to the center of spherical symmetry. After substitution of (16), (17) in (15) with accounting for (12) one can obtain:

$$E_a^2(\mathbf{r})R\left(d\gamma\right)^2\frac{d\theta}{dp}\sqrt{n^2(D)D^2 - p^2}\sqrt{n^2(R)R^2 - p^2}\sin\theta = const = C \tag{18}$$

The refractive attenuation $X(\mathbf{r})$ can be defined as a ratio of intensities of radio wave in the medium and in free space:

$$X(\mathbf{r}) = \frac{E_a^2(\mathbf{r})}{E_0^2(\mathbf{r})} \tag{19}$$

where $E_0(\mathbf{r})$ is the radio field emitted by the same transmitter in free space. The radio field $E_0(\mathbf{r})$ can be described by a relationship:

$$E_0^2(\mathbf{r}) = \frac{C_T}{R_0^2} \tag{20}$$

where R_0 is the distance from the transmitter to the current point $\mathbf{r}$, and C_T is constant which can include the transmitter's power and antenna gain. Substitution (19), (20) in (18) gives:

$$C_T \frac{X(\mathbf{r})}{R_0^2} R \frac{d\theta}{dp} \sqrt{n^2(D)D^2 - p^2} \sqrt{n^2(R)R^2 - p^2} \sin\theta \left(d\gamma\right)^2 = C \tag{21}$$

The next relationships connect central angle θ, impact parameter p, bending angle $\xi(p)$, and distance R_0:

$$\theta = \pi + \xi(p) - \sin^{-1}\frac{p}{n(R)R} - \sin^{-1}\frac{p}{n(D)D} \tag{22}$$

$$\theta = \xi(p) + \sin^{-1}\frac{p}{n(R)R} - \sin^{-1}\frac{p}{n(D)D} \tag{23}$$

$$\frac{R}{R_0}\sin\theta = \sin\gamma, \text{ if } R_0 \to 0 \tag{24}$$

Formula (23) is valid when the tangent point on the ray trajectory, where the ray is perpendicular to the gradient of refractivity, is absent [20]. Equations (22)-(24) allow transforming the formula (21):

$$X(\mathbf{r})\left|\frac{d\xi}{dp}\frac{\sqrt{n^2(D)D^2 - p^2}\sqrt{n^2(R)R^2 - p^2}}{R_0} - \frac{\sqrt{n^2(R)R^2 - p^2} \pm \sqrt{n^2(D)D^2 - p^2}}{R_0}\right| C_T d\Omega = C \tag{25}$$
$$d\Omega = \sin\gamma \left(d\gamma\right)^2$$

where $d\Omega$ is the solid angle occupied by the ray tube.

Constant C can be determined from (25) by estimating the refractive attenuation near the transmitter, when $R_0 \to 0$ (in equation (25) one should choose the lower sign). When $R_0 \to 0$ $X(\mathbf{r})$ is assumed to be equal to unity, i.e. $E_a^2(\mathbf{r}) = E_0^2(\mathbf{r})$, $R_0 \to 0$. This requires that the production of the antenna gain and emitted power along the ray *GTL* C_T (20) does not

change after the installation of the transmitter from free space in a medium with the refractive index $n(D)$. Under these conditions one can obtain from (25) when $R_0 \to 0$:

$$C = C_T n(D) d\Omega \tag{26}$$

Thus the refractive attenuation can be evaluated from (25) and (26) as:

$$X(\mathbf{r}) = \frac{R_0^2 n(D) D \sin\gamma}{RD\sin\theta \left| \frac{d\xi}{dp} \sqrt{n^2(D)D^2 - p^2} \sqrt{n^2(R)R^2 - p^2} - \sqrt{n^2(R)R^2 - p^2} \pm \sqrt{n^2(D)D^2 - p^2} \right|} \tag{27}$$

$$X(\mathbf{r}) = \frac{pR_0}{p_s \sqrt{n^2(D)D^2 - p^2} \sqrt{n^2(R)R^2 - p^2} \left| \frac{d\theta}{dp} \right|}; \; p_s = \frac{RD\sin\theta}{R_0}; \; p = n(D)D\sin\gamma \tag{28}$$

The refractive attenuation $X(\mathbf{r})$ represented by (27) and (28) satisfies the mutuality principle and does not depend on changing locations of the transmitter and receiver.

Previously refractive attenuation $X_p(\mathbf{r})$ has been defined as a ratio of the power flows in the medium and in free space. The magnitude of $X_p(\mathbf{r})$ has been obtained in the form [20]:

$$X_p(\mathbf{r}) = \frac{pR_0}{p_s \sqrt{D^2 - p^2} \sqrt{R^2 - p^2} \left| \frac{d\theta}{dp} \right|} \tag{29}$$

where p_s is the impact parameter corresponding to the line of sight GL. The difference between $X_p(\mathbf{r})$ (29) and $X(\mathbf{r})$ (28) consists in accounting for the refractivity near the transmitter and receiver.

Equations (28) for the refractive attenuation generalize the relationship (29) for the case when the transmitter and receiver are located in a spherically symmetric inhomogeneous medium. This relationship can be appropriate for RO data analysis during experiments provided in the planetary and Earth's atmospheres and ionospheres.

3. Total absorption

A new important relationship between the second-order time derivative (acceleration) of the phase path (eikonal), Doppler frequency, and intensity variations of the radio occultation (RO) signal has been established by theoretical considerations and experimental analysis of the radio-holograms recorded onboard of the CHAMP and FORMOSAT-3 satellites [4, 6-8]. The detected relationship makes it possible to convert the eikonal acceleration (or the time derivative of the Doppler frequency shift) measured using the RO phase data into the refractive attenuation and then exclude it from the RO amplitude data to obtain the total

absorption. The method of measuring of the total absorption from joint analysis of the RO amplitude and phase variations is described below.

Layout of a RO experiment in the transionospheric link using the high-stability, synchronized by atomic-clock, radio signals of GPS navigation system is shown in Figure 2. Point O is the center of spherical symmetry of the Earth's atmosphere. The radio waves emitted by a GPS satellite located at point G enter the receiver input onboard a low-orbit satellite (point L) upon passage along the GTL ray, where T is the perigee of the ray. At point T, the distance h from the ray to the Earth's surface is minimal and the gradient of the refractive index $N(h)$ is perpendicular to the trajectory GTL (Figure 2). Projection of the point T on the Earth's surface determines the geographic coordinates of the studied region. Records of signals along the trajectory of a low-orbit satellite at two frequencies, $f_1 = 1575.42$ MHz and $f_2 = 1227.6$ MHz, are one-dimensional radio-holograms, which contain the amplitudes $A_1(t)$ and $A_2(t)$,

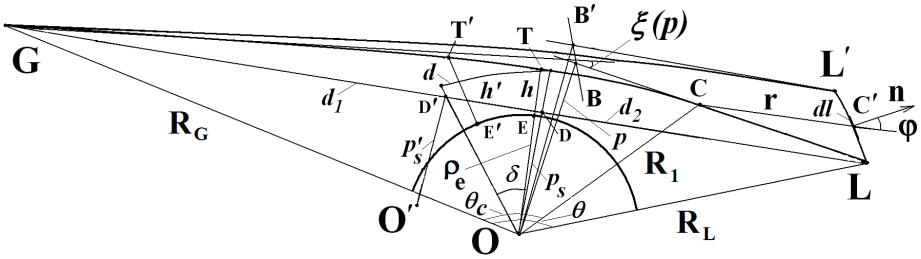

Figure 2. Main geometrical parameters describing the RO experiment conditions.

and the eikonal increments $\Phi_1(t)$ and $\Phi_2(t)$ of a radio field. The vertical velocity of the radio occultation ray in the perigee amounts to about 2 km/s, which is significantly greater than the velocities of motion of layers in the ionosphere and the atmosphere. Thus, the RO data are the instantaneous one-dimensional radio-holograms of the ionosphere and atmosphere. In the case of global spherical symmetry of the ionosphere and atmosphere, the following relations between the phase-path increments $\Phi(t)$ and the refractive attenuation $X(t)$ of radio waves [4-8] are fulfilled:

$$\lambda \frac{dF_d(t)}{dt} = m\frac{d^2\Phi(t)}{dt^2} = ma = 1 - X \tag{30}$$

where λ is the wavelength, $F_d(t)$ is the Doppler frequency of RO signal. In the RO experiments, parameter m can be determined from the orbital data.

Equations (30) relate the refractive attenuation $X(t)$ and the eikonal acceleration a in a form similar to the classical-dynamics equation. Equations (30) determine equivalence of the acceleration of the eikonal a to the time derivative of the Doppler shift $F_d(t)$ and the refractive attenuation $X(t)$. Thus, Eq. (30) make it possible to convert the eikonal

acceleration and/or time derivative of the Doppler shift $F_d(t)$ into the refractive attenuation $X(t)$. This is important for estimation of the total absorption in the atmosphere.

The attenuation of intensity of radio waves $X_a(t)$ can be determined from the amplitude data in the form of a ratio of the intensity $I_a(t)$ of a radio signal propagating across the atmosphere to its intensity $I_s(t)$ in free space:

$$X_a(t) = \frac{I_a(t)}{I_s(t)} \tag{31}$$

The experimental quantity $X_a(t)$ is the product of the refractive attenuation $X_p(t)$ and the total absorption coefficient $\Gamma(t)$ and depends on the gain calibration errors of transmitter and receiver. However, the eikonal acceleration depends only on the refractive attenuation $X_p(t)$. This makes it possible to determine the atmospheric absorption $\Gamma(t)$ for a sufficiently stable level of the amplitude from the relations where $X(t)$ is the refractive attenuation of radio waves which was converted from the eikonal data. Parameter m can be found from the data describing the relative motion of the GPS satellite and the low-orbit satellite with respect to the spherical-symmetry center - point *O* (Figure 2) in the *GOL* plane. The quantity $X(t)$ calculated from Eq. (1) can be used to remove the refractive attenuation effect from the amplitude data:

$$\Gamma = 1 - \frac{X_a(t)}{X(t)} \tag{32}$$

Eqs. (30) - (32) permit one to estimate the total absorption of radio waves Γ along the ray GTL by amplitude and phase measurements of the radio-holograms.

The results of estimation of the total absorption Γ as a function of the altitude in the atmosphere for the experiment onboard the CHAMP satellite (No. 0159 at 14:54 UT) are shown in Figure 3. The experiment has been performed in June 16, 2003. Experiment corresponds to a polar region with geographical coordinates 83.0 N 258.6 W. The refractive attenuations $X_a(h)$ and $X(h)$, which were calculated from the RO amplitude and phase data using Eqs. (1) and (2) are shown in Figure 3 on the left (curves *1* and *2*, respectively). Smooth curves *3* on the left in Figure 3 show the approximation obtained by a least-squares method. Slow trends in the refractive attenuations $X_a(h)$ are practically coinciding and vary from 0 dB at altitudes greater than 34 km to $-$(10–15) dB at altitudes of about 5 km as seen in Figure 3 (left panel). This is experimental proof of the fulfillment of the relations described by Eqs. (1) that have been used for calculation of the refractive attenuation $X(h)$ from the RO phase-channel data of the satellite radio-holograms. Significant correlation between the high-frequency part of the variations in $X(h)$ and $X_a(h)$ takes place (Figure 3). Good correspondence between the variations in $X(h)$ and $X_a(h)$ exists at altitudes of 5 to 32 km

(Figure 3, left panel). At altitudes greater than 30 km, variations in $X_a(h)$ are greater than those in $X(h)$. This difference can be related to possible variations in the receiver (transmitter) gain or, which is more probable, to the ionospheric scintillation effect. The scintillation index S4 was equal to 2.7% in the experiment, and such a value corresponds to moderately disturbed conditions in the ionosphere. Relationships between the refractive attenuations retrieved from the amplitude and phase variations are important for estimation of the altitude dependence of the total absorption in the atmosphere. This dependence is shown by curve *1* in Figure 3 (right panels). Smooth curve *2* corresponds to the total absorption Γ found by a least-squares method, its value nearly corresponds to the absorption in atmospheric oxygen in accordance with [21]. Calculations show that the influence of the absorption in atmospheric oxygen can be tangible at altitudes less than 15 km. Experimental data agree, on the average, with this conclusion.

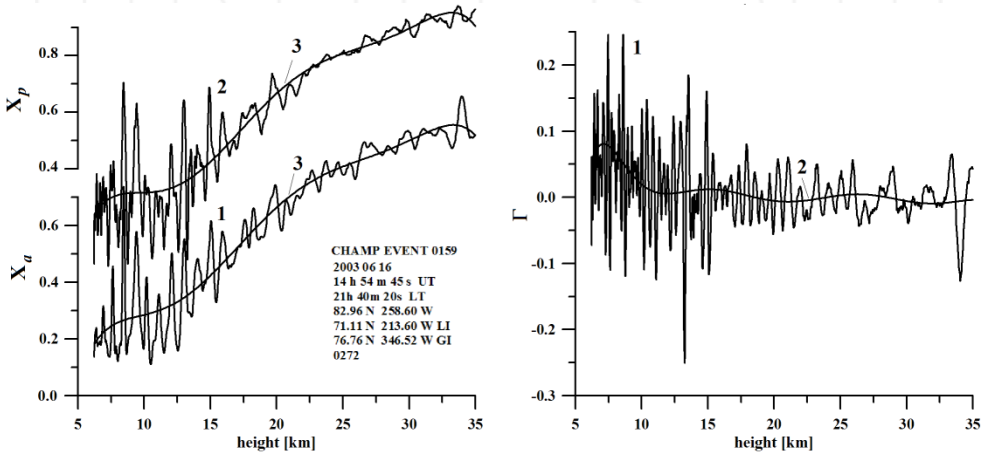

Figure 3. Left. Comparison of the refractive attenuation $X(h)$ retrieved from the eikonal data and attenuation $X_a(h)$ found from the intensity variations of the RO signal. Right. Difference of the refractive attenuations $X - X_a$ (curve 1) and absorption coefficient Γ found by a least-squares method (curve 2).

Obtaining more exact information on total absorption requires averaging of significant variations in the experimental values of Γ. For obtaining the dependence $\Gamma(h)$, the vertical profiles $X(h)$ and $X_a(h)$ were approximated by polynomials using a least-squares method. In Figure 4, left panel, curves *1–5* correspond to the resulting vertical profiles $X(h)$ and $X_a(h)$, and curves *6–10*, Figure 4, middle panel, are related to the dependences $\Gamma(h)$ for five radio-occultation sessions performed using the CHAMP satellite in June 16, 2003. For convenience, curves *1–4*, *6, 7, 9, 10* were displaced for comparison along the vertical axis. All sessions (No. 122, 02:27 LT, 77.6 N 141.0 W; No. 173, 17:35 LT, 80.9 N 337.1 W; No. 0030, 20:59 LT, 77.9 N 83.5 W; No. 0159, 21:40 LT, 83.0 N 258.6 W; and No. 0203, 16:56 LT, 76.3 N

37.9 W) correspond to the north polar regions. At altitudes between 12 and 30 km, the profiles $X(h)$ and $X_a(h)$ almost coincide. At altitudes less than 12 km, splitting of the curves $X_a(h)$ and $X(h)$ (e.g., the curves *a* and *p*, Figure 4, left panel), which begins at different heights, is observed. This effect is notable for all curves *6–10* in Figure 4 (middle panel). The differences at the initial height of splitting can be related to slow variations in the radio signal amplitude. The existence of splitting is probably a signature of the presence of small, but tangible integral atmospheric absorption, whose magnitude is, on the average, close to the values mentioned in [21] and to the magnitude 0.0096 ± 0.0024 dB/km of absorption per unit length measured in [12, 13, 22] (curves *6–10*). The total absorption is varied within the limits 0.034 – 0.081 in the altitude range 12–5 km (Figure 4, middle panel, curves *6–10*). The total absorption is near zero at the altitudes greater 12-15 km. The estimated value of the absolute statistical and systematic errors in the total absorption Γ is ± 0.01.

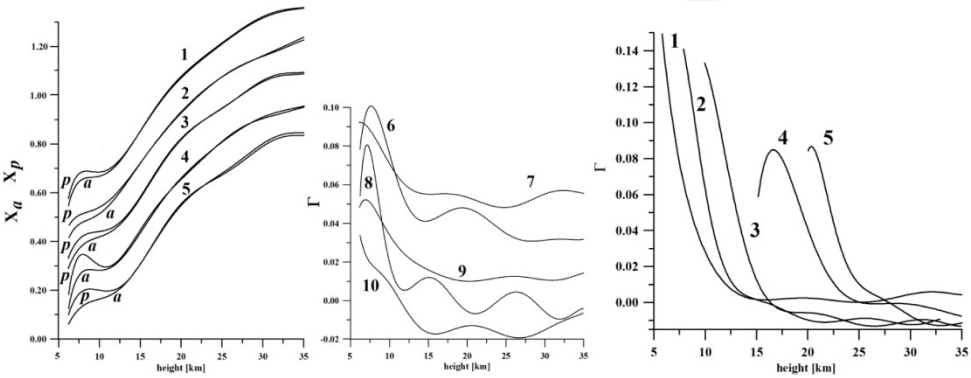

Figure 4. Left and middle panels. Comparison of the refractive attenuation $X(h)$ (index "p") retrieved from the eikonal data and attenuation $X_a(h)$ (index "a") found from the intensity variations of the RO signal (curves 1-5). Curves 6-10 in the middle panel describe the total absorption Γ calculated using Eq. (3). Curves 6,7, and 9,10 are displaced for convenience of comparison. The minimal and maximal values of parameter are: curve 6 -0.01, 0.062; curve 7 -0.001, 0.043; curve 8 -0.01, 0.081; curve 9 -0.0064, 0.0336; curve 10 -0.002, 0.046. Right panel. Averaged values of the total absorption in the Earth's atmosphere found for five days (Curves 1 – 5 correspond to found from CHAMP RO data averaged during February 24; June 16; May 03; November 30; July 07, 2003, respectively).

In Figure 4 (right panel) the averaged values of the total absorption Γ in the Earth's atmosphere are presented for five different days. These values have been found by the introduced eikonal/intensity method from CHAMP RO data for five days: February 24; June 16; May 03; November 30; July 07, 2003, respectively. According to Figure 4 (right panel), the maximal values of the total absorption Γ are containing for different days in the range 0.06 – 0.14 and correspond to the altitudes interval 6 km – 8 km. Averaging significantly reduces the statistical error of measurements, however the systematic errors remain. The systematic errors can be estimated from Figure 4 using negative values of the total absorption Γ as $\pm$

0.01. Analysis of experimental data shows that additional attenuation as compared with the theoretical dependence can exist at altitudes smaller than 8 km. This can be related to the absorption effect in clouds and water vapor.

The introduced method is a perspective tool for investigation of seasonal and annual variations and geographical distributions of the total absorption from RO data. Also this method is, possibly, may be applied to study the influence of the tropical hurricanes and typhoons on the altitude profiles of water vapor in the stratosphere and tropopause.

4. Locality principle and RO remote sensing

A possibility to find the total absorption from joint analysis the RO amplitude and phase data described in section 3 is an important consequence of general locality principle valid in the of RO remote sensing of spherical symmetric atmospheres and ionospheres of the Earth and planets. Up to now this principle is implicit unformulated property of the RO method.

Below the fundamental principle of local interaction of radio waves with a spherically symmetric medium is formulated and introduced in the RO method of remote sensing of the atmosphere and ionosphere of the Earth and planets.

In accordance with this principle, the main contribution to variations of the amplitude and phase of radio waves propagating through a medium makes a neighborhood of a tangential point where gradient of the refractive index is perpendicular to the radio ray.

A necessary and sufficient condition (a criterion) is established to detect from analysis of RO data the displacement of the tangential point from the radio ray perigee.

This criterion is applied to the identification and location of layers in the atmosphere and ionosphere by use of GPS RO data. RO data from the CHAllenge Minisatellite Payload (CHAMP) are used to validate the criterion introduced when significant variations of the amplitude and phase of the RO signals are observed at RO ray perigee altitudes below 80 km.

The detected criterion opens a new avenue in terms of measuring the altitude and slope of the atmospheric and ionospheric layers. This is very important for the location determination of the wind shear and the direction of internal wave propagation in the lower ionosphere, and possibly in the atmosphere.

The new criterion provides an improved estimation of the altitude and location of the ionospheric plasma layers compared with the back-propagation radio-holographic method previously used.

4.1 Application of GPS RO method to study the atmosphere and ionosphere

The radio occultation (RO) method employs the highly-stable radio waves transmitted at two GPS frequencies $f_1 = 1575.42$ MHz and $f_2 = 1227.60$ MHz by the GPS satellites and recorded at a GPS receiver onboard low Earth orbiting (LEO) satellite to remote sense the Earth's ionosphere and neutral atmosphere [4,5,10,11,17,23-42,46,47,52-56,59-61]. When

applied to ionospheric investigations the RO method may be considered as a global tool and can be compared with the global Earth- and space-based radio tomography [42,43]. The RO method delivers a great amount of data on the electron density distribution in the upper and lower ionosphere that are important sources for modernizing the current information over the morphology of the ionosphere and ionospheric processes [44,45]. The RO method has been actively used to study the global distribution of sporadic E-layers in dependence of latitude, longitude, altitude and local time [5, 27-32,39-41,45-47]. These investigations have produced useful data on climatology and the formation process of sporadic E-layers which depend mainly on the Earth's magnetic field and meteor impact according to the theory of the wind shear mechanism of plasma concentration [48-51]. The thermospheric wind and atmospheric tides seem to be the main energy sources for this mechanism [39].

Therefore the spatial distributions of sporadic E layers are important for investigating the connections of natural processes in the neutral and ionized components of the ionosphere. The location and intensity of sporadic E-layers plays a critical role for the quality of radio communications in the HF frequency band. The RO measurements in the atmosphere can be affected significantly by ionospheric contributions since the RO signals propagate through two different parts of the ionosphere.

Usually the ionospheric influence in the RO measurements may be described through a relatively slow change in the excess phase without noticeable variations in the amplitude of RO signals. This effect can be effectively reduced by a number of different methods of ionospheric correction [10,52,53].

However disturbed ionosphere may significantly change not only the phase but also the amplitude of the RO signals. Strong amplitude and phase frequency dependent variations in the RO signals are often surprisingly observed within the altitudes of the RO ray perigee $h(T)$ between 30 and 80 km above the main part of the neutral atmosphere and below the E-layer of the ionosphere. The effects of strong phase and amplitude variations of the RO signals at a low altitude provide a good source of information for the remote sensing of the atmosphere and ionosphere including detecting and studying the internal gravity waves propagating in the atmosphere and ionosphere [54]. Accurate knowledge of spatial location, height and inclination of the sporadic E-layers is important for the estimation of the off-equatorial height-integrated conductivity [44,45]. The RO low altitude amplitude variations have been interpreted as a contribution from the inclined ionospheric layers displaced relative to the RO ray perigee, and equations for the determination of the height and slope of inclined plasma layers from the known displacement of layers have been developed [27].

The altitudes of sporadic E-layers have been evaluated as the height of the RO radio ray perigee in recent times [28,39-41]. A relationship between the eikonal (phase path) and amplitude variations in the GPS/MET RO data has been analyzed in [53] and conclusions have been made that (i) the amplitude variations in distinction to the phase of RO signal have a strong dependency on the distance from observation point to the location of an ionospheric irregularity and (ii) the location of the irregularities in the low ionosphere may be determined by measuring the distance between the observation point up to a phase screen which should be located perpendicularly to the RO ray trajectory at its perigee.

A radio-holographic back-propagation method has been suggested and applied for location of the irregularities in E- and F-layers of the ionosphere [10,11]. A relationship between the derivatives of the phase, eikonal, Doppler frequency on time and intensity of radio waves propagating through the near Earth's space has been detected from both theoretical considerations and experimental analysis of the RO radio-holograms [4,5,31,36-38,47]. The introduced eikonal acceleration technique can de used for locating layers in the ionosphere and atmosphere.

The aim of this section is to demonstrate the possibility of identifying the contributions and measuring parameters of the inclined plasma layers by means of an analytical criterion. A test of a suggested method is provided by use of CHAMP RO data.

4.2. Criterion for layer locating

The scheme of RO experiments is shown in Figure 2. A navigational satellite G emitted highly-stable radio waves which after propagation through the ionosphere and atmosphere along the radio ray GTL arrived to a receiver onboard the Low Earth Orbital (LEO) satellite L. The amplitudes and phase variations of the RO signals are recorded as a function of time, sent to the ground stations with orbital data and analyzed with an aim to find the physical parameters of the neutral atmosphere and ionosphere along the trajectory of the RO radio ray perigee – point T (Figure 2). The receiver onboard LEO records the amplitude $A_1(t)$, $A_2(t)$ and the excess phase path $\Phi_1(t)$, $\Phi_2(t)$ of the GPS transmitted radio wave signals as a function of time t at two GPS frequencies.

The global spherical symmetry of the ionosphere and atmosphere with a common centre of symmetry is the cornerstone assumption of the RO method. Under this assumption a small area centered at tangent point T (Figure 2) where the RO ray is perpendicular to the gradient of refractivity, makes a significant contribution to the amplitude and phase variations of RO signals despite the prolonged path GTL (Figure 2). Under the global spherical symmetry condition the tangent point coincides with the RO ray perigee T. The size of this area along the ray GTL is equal to the horizontal resolution of the RO method $\Delta_h = 2\left(2l_f\rho_e\right)^{1/2}$, where $l_f = \left(\lambda d_2\right)^{1/2}$ is the size of the Fresnel zone, λ is the wavelength, ρ_e is the distance TO, d_2 is the distance TL which is nearly equal to DL (Figure 2). The magnitude of Δ_h corresponds to the minimal horizontal length of a layer estimated by the RO method.

The quiet ionosphere introduces regular trends in the excess phases at two GPS frequencies which can be removed by the ionospheric correction procedure [25,53]. The contributions in the phase and amplitude variations of RO signals of the intensive sporadic E-layers at the altitude interval 90-120 km is significantly greater than the impact of the F-layer turbulent structures [25]. Impact of a regular layer on the RO signal depends on position relative to the RO ray perigee. The length, $l_{c\varepsilon}$, of coherent interaction of the RO signal with a layer having the vertical width l depends on the elevation angle ε between the local horizon

direction and ray trajectory: $l_{c\varepsilon} \approx \frac{l}{\sin\varepsilon}$. For the RO ray perigee the elevation angle, ε, is zero, and the corresponding value l_c is described by relationship:

$$l_c = 2(2l\rho_e)^{1/2} \tag{33}$$

The ratio G of the lengths l_c and $l_{c\varepsilon}$ is equal to:

$$G = \frac{l_c}{l_{c\varepsilon}} = 2\sqrt{\frac{2\rho_e}{l}}\sin\varepsilon \tag{34}$$

Under spherical symmetry condition $\sin\varepsilon$ is about 0.25 at the altitude of ionospheric F-layer 250 km, and one can obtain from (34):

$$G \approx 0.5\sqrt{\frac{2\rho_e}{l}} \approx \frac{0.57\cdot 10^2}{l^{1/2}} \tag{35}$$

If the vertical width l is about one kilometer, the contribution to the phase variations of a layer disposed in the RO ray perigee differs by about a hundred times on the impact of the similar layer located in the F-region. Therefore as a rule the RO method is effective tool for layers detection and measurements of their parameters with high vertical resolution and accuracy along of the trajectory of the RO ray perigee.

The next connection between the excess phase path (eikonal) $\Phi(t)$ acceleration a and the refractive attenuation of electromagnetic waves $X_p(t)$ have been detected and validated [4,5,31,36-38]:

$$1 - X_p(t) = ma,\ a = \frac{d^2\Phi(t)}{dt^2},\ m = d_2(1 - d_2 / R_0) / (dp_s / dt)^2 \tag{36}$$

where d_2, R_0 are the distances along the straights lines DL and GL, respectively, p, p_s are the impact parameters corresponding to the ray GTL and the straight line GL (Figure 1). Note, that the distance d_2 is nearly equal to distance TL within an accuracy corresponding to the horizontal resolution of the RO method (about 100-300 km). Parameters m and dp_s/dt may be evaluated from the orbital data. The first formula (36) has been derived under condition [37]:

$$\left|(p - p_s)\frac{dR_{1,2}}{dt}\right| \ll \left|p_s\frac{dp_s}{dt}\right| \tag{37}$$

where R_1, R_2 are the distances OG, OL, respectively, (Figure 1). Condition (37) holds for RO studies of the atmospheres and ionospheres of the Earth and planets because the module of difference $p - p_s$ is always well below the magnitudes of p, p_s. If absorption is absent the magnitude $X_p(t)$ describes the refractive attenuation determined from the amplitude data:

$$X_p(t) \equiv X_a(t) \tag{38}$$

$$X_a(t) = I / I_0 \tag{39}$$

where I_0, I are the intensities of the RO signals measured before and after the immersion of the RO ray in the atmosphere, respectively. It should be noted that the total absorption in the atmosphere can be determined by excluding the refractive attenuation found from measurements of the eikonal acceleration at the same frequency by use of the first Eq. (36).

$$\Gamma = 1 - X_a(t) / X_p(t) \tag{40}$$

Eqn. (36) and (40) are the basis of the proposed method for determining the total absorption by measuring the time dependence of the intensity and eikonal of the RO signal at one frequency [31]. This method is much simpler than the previously used method based on estimation of the refractive attenuation on the first derivative of the bending angle on the impact parameter. When the total absorption is absent, it follows from (36) and (38), if the center of symmetry is located at point O :

$$1 - X_p(t) \equiv 1 - X_a(t) = ma \tag{41}$$

Relationship (41) establishes equivalence of the values $X_p(t), X_a(t)$ in the case of the spherical symmetry with centre O . Criterion (38) is a necessary and sufficient condition to ensure that the tangential point coincides with the radio ray perigee. This criterion is valid when the total absorption is absent and the requirement of the global spherical symmetry is fulfilled. In this case variations of the refractive attenuations found from the phase and amplitude variations of the RO signal should be the same at any time and can be attributed to the influence of the medium near the ray perigee (the locality principle). Therefore the RO method is based on an implicit locality principle and the RO method results correspond to the trajectory of motion of the RO ray perigee in the case of a spherically symmetric medium.

However the locality principle has more general meaning. Therefore it is necessary to extend the theory of the RO method to develop an appropriate technique to find the locations of the tangent points on the RO ray. This is an aim of the last part of this section.

In some cases the centers of spherical symmetry in the two parts of the ionosphere located on the path GTL (Figure 2) do not coincide with that of the neutral atmosphere [4,31,32,46,47]. In particular, this effect can be caused by the displacement of the centre of spherical symmetry O' of an ionospheric part of the ray GTL from the point O (Figure 2). In this case according to the derivation made previously [37] the inequality (37) is also valid after changing the distances $R_{1,2}$ to $R'_{1,2}$ and impact parameters p, p_s to p', p'_s because smallness of the difference $p' - p'_s$ as compared with any of the values p', p'_s . Therefore the identity (38) is valid also in the new coordinate system with centre at point O' (Figure 2):

$$X_p'(t) \equiv X_a(t) \tag{42}$$

where $X_p'(t)$ - is a new value of the refractive attenuation relevant to a new center of spherical symmetry:

$$1 - X_p'(t) = m'a,\ a = \frac{d^2\Phi(t)}{dt^2},\ m' = d_2'(1 - d_2' / R_0) / (dp_s' / dt)^2 \tag{43}$$

where m' - is a new value of the parameter m relevant to a new center of spherical symmetry O', d_2' is the distance $D'L$, respectively (Figure 2). As compared with formula (36) the first equation (43) is different with new values of the refractive attenuation $X_p'(t)$ and parameter m'. The refractive attenuation $X_a(t)$ found from the amplitude data (39) and the eikonal acceleration a do not depend on location of the spherical symmetry centre. Identity (42) extends the criterion (38) to general case in which the centre of spherical symmetry is shifted to an arbitrary point.

This allows one to formulate the locality principle for remote sensing of layered spherically symmetric medium in the absence of absorption. A certain point of the radio ray is tangential if and only if the refractive attenuations found from the second derivative of the eikonal on time and intensity variations of the radio waves passed through the medium are equal. In this case both the intensity and the second derivative of the eikonal variations are mainly influenced by a small neighbourhood of the tangential point.

The principle of locality allows one to determine the location of a tangential point and to find the altitude, slope and displacement of a layer from the radio ray perigee. According to Eqn. (36), (43) it follows:

$$1 - X_a(t) \equiv \frac{m'}{m}(1 - X_p) \tag{44}$$

where the refractive attenuation X_p is determined from Eq. (33) using measured value a; coefficients m', m - correspond to the centres of spherical symmetry O and O'. It follows from (36), (43), (44):

$$X_p - X_a(t) = \left(\frac{m'}{m} - 1\right)(1 - X_p) = \left[\frac{d_2'(1 - d_2' / R_0)(dp_s / dt)^2}{d_2(1 - d_2 / R_0)(dp_s' / dt)^2} - 1\right](1 - X_p) \tag{45}$$

If the displacement of the center of spherical symmetry satisfies the following conditions:

$$d_2 / R_0,\ d_2' / R_0 \ll 1;\ \ \frac{dp_s}{dt} \approx \frac{dp_s'}{dt} \tag{46}$$

then one can find from (45):

$$X_p - X_a(t) = \frac{d_2' - d_2}{d_2}(1 - X_p) = \frac{d}{d_2}(1 - X_p) \tag{47}$$

where d is the distance DD' (Figure 2). In the case of small refraction effect the distance d is approximately equal to the length of arc TT'. Relationship (47) establishes a natural connection between the displacement of the tangential point from the radio ray perigee d and variations of the refractive attenuations $X_a(t)$ and X_p.

Let us consider the refractive attenuation variations as the analytical signals in the form:

$$1 - X_p(t) = ma = A_p(t)\mathrm{Re}\left[\exp j\chi_p(t)\right];\ 1 - X_a(t) = A_a(t)\mathrm{Re}\left[\exp j\chi_a(t)\right] \tag{48}$$

where $A_p(t)$, $A_a(t)$; $\chi_p(t)$, $\chi_a(t)$ are, correspondingly, the amplitudes and phases of the analytical signals, relevant to the functions $1 - X_p(t)$ and $1 - X_a(t)$. The amplitudes and phases $A_p(t)$, $A_a(t)$; $\chi_p(t)$, $\chi_a(t)$ describe atmospheric (ionospheric) modulations of the refractive attenuation variations $1 - X_p(t)$ and $1 - X_a(t)$. The phases $\chi_p(t)$, $\chi_a(t)$ differ from the excess phase path (eikonal) $\Phi(t)$. In the case when the variations $1 - X_p(t)$ and $1 - X_a(t)$ can be described by a narrowband process the functions $A_p(t)$, $A_a(t)$; and $\chi_p(t)$, $\chi_a(t)$ can be found by the numerical Hilbert transform or by other methods of the digital data analysis.

After substitution (48) in (44) one can obtain:

$$A_a(t)\mathrm{Re}\left[\exp j\chi_a(t)\right] \equiv \frac{m'}{m}A_p(t)\mathrm{Re}\left[\exp j\chi_p(t)\right] \tag{49}$$

The ratio $\frac{m'}{m}$ is supposed to be nearly constant during the RO measurement event. For fulfilling (49) the phases $\chi_p(t)$ and $\chi_a(t)$ should be equal, but the amplitudes $A_a(t)$ and $A_p(t)$ are different. In this case one can obtain from (49) under the conditions (46) an alternative relationship for the displacement d in the form:

$$d = d_2' - d_2 = d_2\frac{A_a - A_p}{A_p};\ d_2 = \sqrt{R_2^2 - p_s^2};\ m' = \frac{A_a}{A_p}m \tag{50}$$

Equation (50) establishes a rule: location of a tangent point on the ray trajectory can be fulfilled using the analytical amplitudes of the refractive attenuation variations $A_{a,p}$; the displacement d is positive or negative depending on the sign of difference $A_a - A_p$, the tangent point T' is located on the parts GT or TL, respectively. The phases $\chi_p(t)$ and $\chi_a(t)$ should be equal within some accuracy determined by a quality of measurements. From the last equation (50) one can find the coefficient m' if the magnitude m is known.

Note, that equation (50) is valid when the distance of one of the satellites from the ray perigee T is many times greater than the corresponding value for the second one. This condition is fulfilled for the planetary RO experiments provided by use of the communication radio link spacecraft-Earth and GPS occultations [31].

Correction to the layer height Δh and its inclination δ with respect to the local horizontal direction can be obtained from the displacement d [27]:

$$\delta = d / \rho_e, \ \Delta h = 0.5 d\delta \tag{51}$$

where ρ_e is the distance TO (Figure 1).

Condition of the spherical symmetry with new center O' justifies application of the Abel's transform for solution of the inverse problem. For the Abel's transform the next formula is used [55]:

$$N(p_0) = -\frac{1}{\pi}\int_{p_0}^{\infty} \ln\left[\frac{p}{p_0} + \sqrt{\left(\frac{p}{p_0}\right)^2 - 1}\right] \frac{d\xi(p)}{dp} dp; \ \frac{dN(p_0)}{dh} = \frac{1 + N(p_0)}{\left(1 - \frac{dN(p_0)}{dp_0}\left(r_e + h\right)\right)} \frac{dN(p_0)}{dp_0} \tag{52}$$

where p_0 is the magnitude of the impact parameter p corresponding to ray GTL in the initial instant of time t_0, $N(p_0)$ and $\frac{dN(p_0)}{dh}$ are the refractivity and its vertical gradient. the derivative of the bending angle $\xi(p)$ on the impact parameter p $\frac{d\xi(p)}{dp}$ can be found from the refractive attenuation X by use of equation obtained previously [20]:

$$\frac{d\xi}{dp} \approx \left(1 - \frac{1}{X}\right) \frac{R_0}{\sqrt{R_1^2 - p^2}\sqrt{R_2^2 - p^2}} \tag{53}$$

where R_0 is the distance GL (Figure 1). from (36), (52), (53) one can obtain the modernized formula for the Abel inversion:

$$N(p_0) = \frac{1}{\pi}\int_{t_0}^{t_x} \ln\left[\frac{p(t)}{p_0} + \sqrt{\left(\frac{p(t)}{p_0}\right)^2 - 1}\right] \frac{m'a}{\sqrt{R_2^2 - p(t)^2}} \frac{dp_s}{dt} dt \tag{54}$$

Factor m' in (54) can be estimated from the last equation (50). Magnitude $m'a$ in (54) may be changed by the value $1 - X_a$ to use directly the RO amplitude data for the Abel inversion.

Note, that equation (52) provides the Abel's transform in the time domain t_0, t_x where a layer contribution does exist. The linear part of the regular trend due to influence of the upper ionosphere is removed because the eikonal acceleration a in (54) contains the second derivative on time. However the influence of the upper ionosphere is existing because it

contributes in the impact parameter $p(t)$. Also nonlinear contribution of the upper ionosphere remains in the eikonal acceleration a. Equation (54) gives approximately that part of the refractivity altitude distribution which is connected with influence of a sharp plasma layer. The electron density vertical distribution in the earth's ionosphere $N_e(h)$ is connected at GPS frequencies with the refractivity $N(h)$ via relationship:

$$N_e(h) = -\frac{N(h) f^2}{40.3} \tag{55}$$

where f is carrier frequency [Hz], $N_e(h)$ is the electron content $\left[\frac{el}{m^3}\right]$.

4.3. Analysis of CHAMP experimental data

To consider a possibility to locate the plasma layers we will use a CHAMP RO event 005 (November 19, 2003, 0 h 50 m UT, 17.3 S, 197.3 W) with strong quasi-regular amplitude and phase variations. The refractive attenuations of the CHAMP RO signals X_a, X_p found from the intensity and eikonal data are shown in Figure 5 (left panel) as functions of the RO ray perigee altitude h. The eikonal acceleration a has been estimated by double differentiation of a second power least square sliding polynomial over a sliding time interval $\Delta t = 0.5\ s$. This time interval corresponds approximately to the vertical size of the Fresnel's zone of ~1 km since the vertical component of the radio ray was ~2.1 km/s. The refractive attenuation X_p is derived from the evaluated magnitude a using equation (36); m value is obtained from the

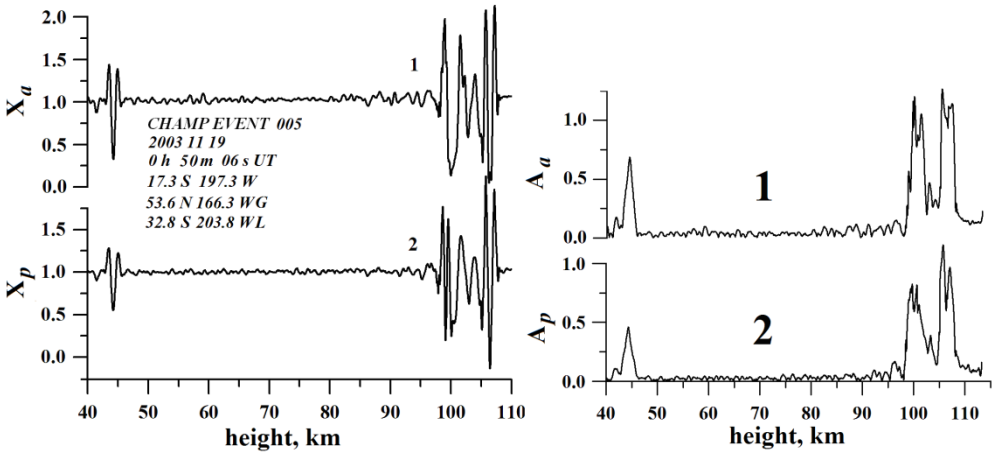

Figure 5. Left plot: the refractive attenuations X_a, X_p found from the intensity and eikonal ro data at frequency f_1 (curves 1 and 2, respectively). Right plot: the amplitudes A_a, A_p of analytical signals corresponding to the variations of the refractive attenuations X_a, X_p (curves 1 and 2).

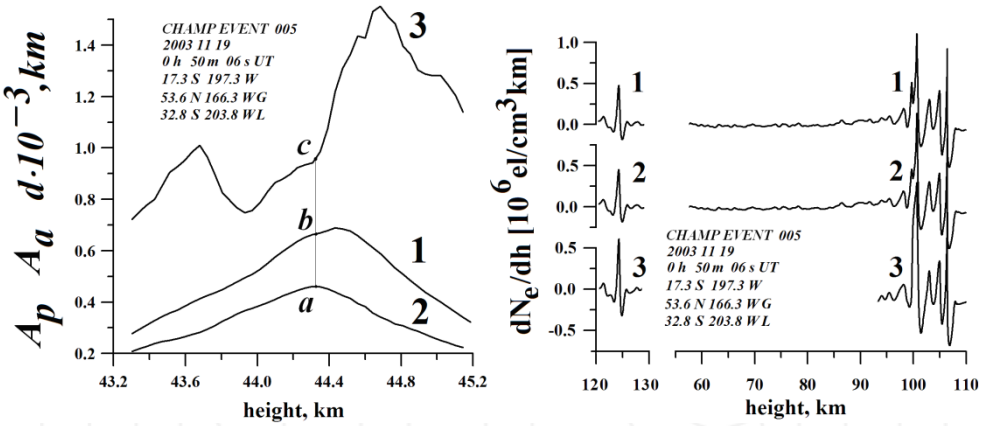

Figure 6. Left: evaluation of the plasma layer displacement from the RO perigee d. Right: results of restoration of the vertical gradients of the electron density.

orbital data. The refractive attenuation X_a is derived from the ro amplitude data by a least square method with averaging in the same time interval of 0.5 s. in the altitude ranges of 42-46 km and 98-106 km, the refractive attenuations variations X_a, X_p are strongly connected and may be considered as coherent oscillations caused by sporadic layers (Figure 5, left panel). Using the Hilbert numerical transform, the amplitudes A_a, A_p of analytical signals related to $X_a - 1$ and $X_p - 1$ have been computed and are shown in Figure 5 (right panel). In the altitude range of 42-46 km, the amplitudes A_a and A_p are nearly identical, but the magnitude of A_a is about 1.5 times greater than that of A_p. Accordingly, a plasma layer is displaced from the RO ray perigee T in the direction to the satellite G (Figure 2). A similar form of variations of the refractive attenuations $X_a - 1$ and $X_p - 1$ allows locating the detected ionospheric layer. The displacement d corresponding to a plasma layer recorded at the 44 km altitude of the RO ray perigee is shown in Figure 6 (left). The curves 1 and 2 in Figure 6 (left) correspond to the amplitudes A_a, A_p. Curve 3 describes the displacement d found from the amplitudes A_a, A_p using equation (50). The changes of d are concentrated in the altitude range of 720-1500 km when the functions A_a, A_p vary near their maximal values of 0.46 and 0.69 in the ranges of $0.2 \le A_p \le 0.46$ and $0.2 \le A_a \le 0.69$ respectively. The statistical error in the determination of the ratio $\frac{A_a - A_p}{A_p}$ in equation (50) is minimal when A_p is maximal. Point a in Figure 6 (left panel) marks the maximum value of A_p, and the points *b* and *c* denote the corresponding values $A_a = 0.67$ and $d = 940\ km$ respectively, the plasma is displaced from the RO ray perigee T in direction to the navigational satellite G (Figure 2). If the relative error in the measurements of A_p is 5%, then, according to Figure 6

(left) the accuracy in the estimation of d is about $\pm 120\ km$. The inclination of a plasma layer to a local horizontal direction calculated using eqns. (51) is approximately equal to $\delta = 10.4° \pm 0.2°$.

The vertical gradient $\frac{dN_e}{dh}$ of the electron density distribution $N_e(h)$ for the given RO event is shown in Figure 6 (right). Curves 1 and 2 correspond to the vertical gradient $\frac{dN_e}{dh}$ retrieved using eq. (52) and (54) respectively. Curve 3 is related to the vertical gradient $\frac{dN_e}{dh}$ retrieved using the refractive attenuation X_a and formula (54). The real altitude of the ionospheric layers is indicated on the horizontal axis in Figure 6 (right). Two ionospheric layers are seen (curves 1, 2, and 3 in Figure 6, right). The first layer is located on the line GT at the 120-130 km altitudes at a distance ~ 950 km from point T. The second layer is located near the RO perigee at the 98-108 km altitudes (Figure 5 and Figure 6, right). From the comparison of the refractive variations X_a, X_p (Figure 5, left) and the vertical gradients of the electron content (Figure 6, right) the width of the sporadic E-layers is nearly equal to the altitude interval of the amplitude variations of the RO signals. From Figure 6 (right), the variations of the vertical gradient of the electron density are concentrated in the interval $-\frac{1.1 \cdot 10^6 el}{cm^3 km} < \frac{dN(h)}{dh} < \frac{1.1 \cdot 10^6 el}{cm^3 km}$. These magnitudes of $N_e(h)$ are typical for intensified sporadic E-layers [45]. The height interval of the amplitude variations is nearly equal to the height interval of the variations in the electron density and its gradient.

The second example of the identification and location of sporadic plasma layer in the lower ionosphere is shown in Figure 7 for CHAMP RO event 211 (July 04 2003, 10 h 54 m LT, 2.1 N, 145.6 W) with intensive sporadic e layers. The refractive attenuations X_a and X_p of the CHAMP RO signals at f_1 obtained from the intensity and eikonal data are shown in Figure 7 (a) as functions of the RO ray perigee altitude h. The refractive attenuations variations X_a, X_p are strongly correlated and can be considered as coherent oscillations caused by a single sporadic e-layer. as shown in Figure 7 (b), the amplitudes A_a, A_p corresponding to $X_a - 1$, $X_p - 1$ are attained from the Hilbert numerical transform and the magnitude A_a is about 1.3 times greater than A_p. This means that a corresponding plasma layer is displaced from the RO ray perigee T in the direction to the satellite g (Figure 1). The displacement d of the tangent point can be determined from the amplitude variations A_a, A_p. The displacement d, the correction of the altitude Δh, the corrected height h' of the plasma layer maximum, and the slope of the plasma layer relative to the horizontal direction δ are shown in Figure 7, c, d. Curves 1, 2 and 3 in Figure 7 (d) are the amplitudes A_a, A_p and the corrected height h' of the plasma layer maximum on the RO ray perigee altitude h respectively. Curves 1, 2 and 3 in Figure 4 (c) are the displacement d (its values are marked

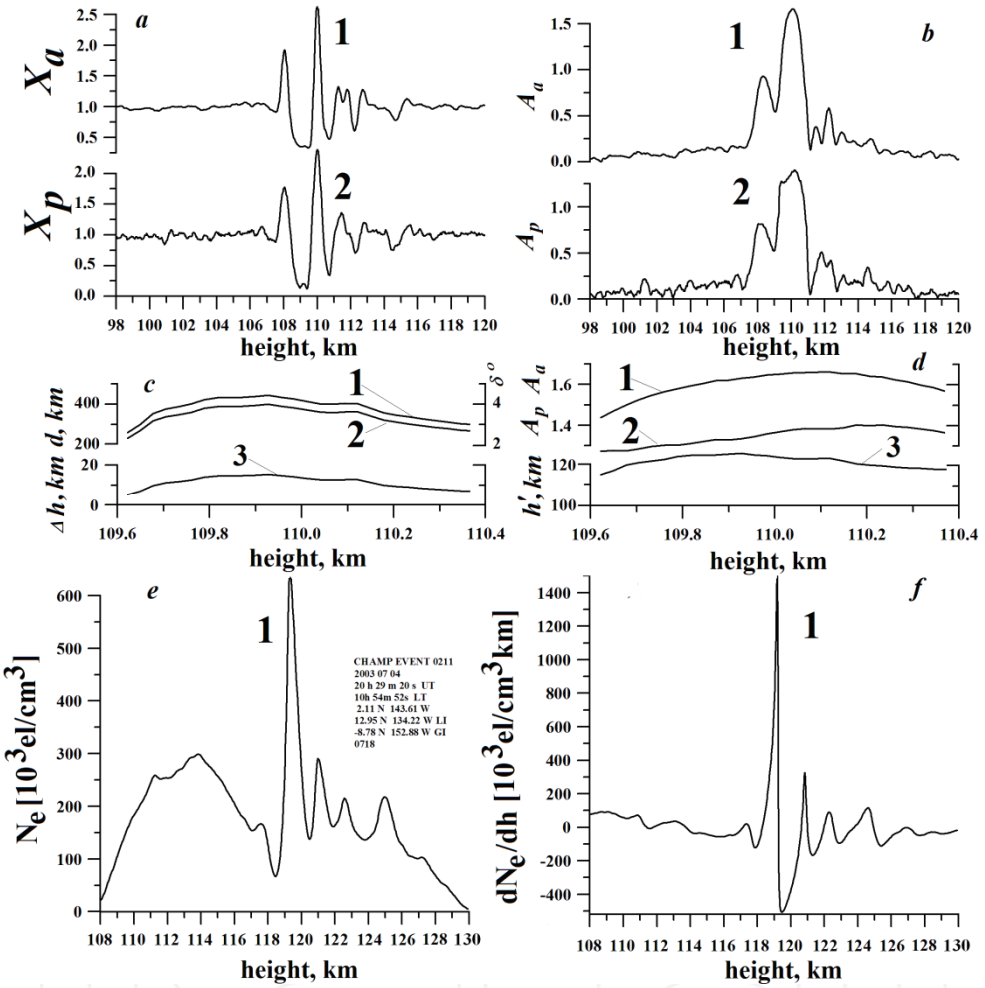

Figure 7. Panels a-d: identification and location of a layer in the lower ionosphere. Panel e: distribution of the electron density in the identified sporadic Es layer. Panel f: distribution of the gradient of electron density.

at the left vertical axis), the layer slope δ [degrees] (right vertical axis), and the correction Δh respectively. the changes of d, Δh, and δ are concentrated in the ranges of 240-400 km, 5-15 km, and 2.2°…3.2° when the altitude of the ro ray perigee changes in the range of 109.6-110.4 km. From these changes the average values of d, Δh, and δ are determined, i.e. $d = 350\ km \pm 50$ km; $\Delta h = 10\ km \pm 5\ km$, and $\delta = 3.1° \pm 0.3°$. It is concluded that the detected sporadic layer is displaced from the ro ray perigee by 350 km in the direction to the gps satellite and the altitude of which is 10 km greater than the height of the point T. The height distribution of the electron density $N_e(h')$ and its altitude gradient $\frac{dN_e(h')}{dh'}$ recalculated from

the modernized Abel inversion equation (54) is shown in Figure 7, e, f. Note, that the function $N_e(h')$ represents the sporadic E-layer contribution with the approximation $N(t_x, p_0) = 0$. This suggests that the above calculation reflects the high-frequency part $N_e(h')$ and with the magnitude of the vertical spatial periods below 10 km. The maximal value of the electron density is located at the height of 119.2 km (Figure 7 e). The maximal gradient of the electron content ~$1.4 \cdot 10^6$ [$el / cm^3 km$] is observed at the altitude of 119.0 km (Figure 7 f). The altitude dependent quantity $N_e(h')$ demonstrates the wave-like structure that is possibly related to the wind shears in the vertical distribution of horizontal wind in the neutral gas [50].

The introduced method appears to have a considerable potential to resolve the uncertainty between the part GT and LT of the ray trajectory and determine the location of the inclined layers. This method accurately indicates the locations of the maximal values and direction of the gradient of the electron density including the distance, altitude and slope. According to existing theory, the maximum of the electron content in sporadic E-layers are usually connected with influence of the wind shear [45]. Therefore the RO method is capable to locate the wind shear in the lower ionosphere. The gradient of the electron content can correspond to the wave fronts of different kinds of wave influencing on the ionospheric plasma distribution [50]. In the case of the internal gravity waves (GW) the inclination of the wave vector to the vertical direction can be used to find the angular frequency of GW [54]. Therefore the introduced criterion and technique extended the applicable domain of RO method. Additional validation of this method through analyzing the CHAMP data and comparison with ground-based ionosonde information is the task for the future work.

4.4. Comparison of the eikonal acceleration/intensity technique with back-propagation radio-holographic methods

The analytic technique can be compared with the radio-holographic approach for locating plasma structure in the ionosphere introduced previously [10,11]. In general the radio-holographic back-propagation may be carried out using a Green function $G(|\mathbf{r}|)$ as a reference signal and a complex field $\phi(l)$ measured along a part of orbital trajectory of a LEO satellite ($L'L$) (Figure 2) [30]:

$$\phi(C) = \left[ik_0 / (2\pi) \right]^{1/2} \int_{LL'} r^{-1/2} G(|\mathbf{r}|)\ \phi(l) \cos\varphi\ dl \tag{56}$$

where $|\mathbf{r}|$ is the distance CC' (Figure 2), $\phi(C)$ is the radio fields restored by a back-propagation method at point C, φ is the angle between the vector $\mathbf{r}$, connecting the observation point C and current integration element dl with center C', and normal $\mathbf{n}$ to the curve $L'L$ (Fig.1).

The Green function $G(|\mathbf{r}|)$ is a solution of the scalar wave equation:

$$(\Delta + k_0^2 n^2(r)) G(\mathbf{r}, \mathbf{r}') = -4\pi\delta(\mathbf{r} - \mathbf{r}') \tag{57}$$

where, k_0 is the module of the wave vector in the free space, $\mathbf{r},\mathbf{r}'$ are the vectors indicating the coordinates of a point in a medium and a source of the field, $n(r)$ is the spatial distribution of the refraction index. It is supposed below that $n(r)$ depends only on a radial coordinate r of layered structures relative to a centre of spherical symmetry.

To obtain the optimal values of the vertical resolution and accuracy in measuring physical parameters in the atmosphere and ionosphere, usually the Green function $G(|\mathbf{r}|)$ in (56) may be chosen in the form depending on the model of a layered medium $n_m(r)$ [30]. As the simplest case of a reference signal, the Green function $G(|\mathbf{r}|)$ describing spherical waves in the free space can be selected [56]:

$$G(|\mathbf{r}|) = \exp(i\pi / 4)\exp(-ik_0|\mathbf{r}|) / |\mathbf{r}|^{1/2} \tag{58}$$

The Green function $G(|\mathbf{r}|)$ corresponding to radio waves emitted by a point source in a spherical symmetric layered medium has been suggested [30]:

$$G(|\mathbf{r}|) = A_G(|\mathbf{r}|,\varphi)\exp(-ik_0\Phi_G(|\mathbf{r}|)) \tag{59}$$

where, $\Phi_G(|\mathbf{r}|)$, $A_G(|\mathbf{r}|,\varphi)$ are the eikonal and amplitude of the Green function $G(|\mathbf{r}|)$.

The complex wave field $\phi(l)$ at the orbital trajectory $L'L$ in the wave-optics approximation is given by relationship [30]:

$$\phi(l)=X^{1/2}(p)\exp\left[ik_0\Phi(p)\right] \tag{60}$$

where, p is the impact parameter depending on the location of the element dl, $X(p)$ is the refractive attenuation along ray GTL. The eikonal $\Phi(p)$ and distance CC' $|\mathbf{r}|$ are presented by the following relationships:

$$\Phi(p) = \sqrt{R_L^2 - p^2} + \sqrt{R_G^2 - p^2} + p\xi(p) + \kappa(p) \tag{61}$$

$$|\mathbf{r}| = \sqrt{R^2 + R_1^2 - 2RR_1\cos(\theta - \theta_c)} \tag{62}$$

where, $\xi(p)$ is the bending angle, $\kappa(p)$ is the main refractivity part depending on the distribution of the vertical gradient of refractivity along the radio ray GTL, R_G, R, and R_1 are the distances OG, OC, and OC', respectively, O is the spherical symmetry center, θ_c is the central angle with the vertex at O between directions OG and OC (Figure 2). The bending angle $\xi(p)$ is the negative derivative of the main refractivity part $\kappa(p)$ with respect to p:

$$\xi(p) = -\frac{d\kappa(p)}{dp} \tag{63}$$

The central angle θ (Figure 2) is connected with the impact parameter p of the ray GTL by the following equation:

$$\theta = \pi + \xi(p) - \sin^{-1}\frac{p}{R_1} - \sin^{-1}\frac{p}{R_g} \tag{64}$$

The back-propagated field $\phi(C)$ may be evaluated by stationary phases. In the case of circular orbits of the transmitting and receiving satellites the integration along the curve $L'L$ for obtaining the field $\phi(C)$ may be provided on the central angle θ. The phase of the back-propagated field in point C is equal to:

$$\psi(p) = \sqrt{R_L^2 - p^2} + \sqrt{R_G^2 - p^2} + p\xi(p) + \kappa(p) - \Phi_G(|\mathbf{r}|) \tag{65}$$

The form of the eikonal $\Phi_G(|\mathbf{r}|)$ depends on the Green functions eqns (58) and (59) used for the back propagation:

$$\Phi_G(|\mathbf{r}|) = |\mathbf{r}| \tag{66}$$

$$\Phi_G(|\mathbf{r}|) = \sqrt{R_1^2 - p_b^2} - \sqrt{n_m^2(R)R^2 - p_b^2} + p_b\xi_m(p_b) + \kappa(p_b) \tag{67}$$

where, the refraction index $n_m(R)$ in point C and the bending angle $\xi_m(p_b)$ are corresponding to the refractivity distribution in a medium for which Green function $G(|\mathbf{r}|)$ (i.e. equation (59)) is known. For Green function (58) $n_m(R) \equiv 1$, $\xi_m \equiv 0$. The central angle $\theta - \theta_c$ is connected with the impact parameter p_b of the back-propagated ray CC' (Figure 2) by:

$$\theta - \theta_c = \xi_m(p_b) + \sin^{-1}\frac{p_b}{n_m(R)R} - \sin^{-1}\frac{p_b}{R_1} \tag{68}$$

The stationary phase method can be applied to evaluate the back-propagating field. For the stationary point, the following equation holds:

$$\frac{\partial\psi}{\partial\theta} = 0 \tag{69}$$

After substitution (65)-(68) into (69) one obtains:

$$\frac{\partial\psi}{\partial\theta} = \frac{\partial\Phi}{\partial p}\frac{\partial p}{\partial\theta} - \frac{\partial\Phi_G(|\mathbf{r}|)}{\partial p_b}\frac{\partial p_b}{\partial\theta} = p\frac{\partial\theta}{\partial p}\frac{\partial p}{\partial\theta} - p_b\frac{\partial(\theta - \theta_c)}{\partial p_b}\frac{\partial p_b}{\partial\theta} = p - p_b = 0 \tag{70}$$

From equation (70) the impact parameters p, p_b related to ray GTL and the back propagated ray CC' are identical in the stationary point C'. Therefore the field $\phi(C)$ is

back-propagating in the occultation plane along the tangents to the occultation rays at any point of the orbital trajectory $L'L$ (Figure 2). The back-propagated rays are the straight lines or curves depending on the form of Green functions (58) or (59) used. The stationary phase method gives the next expression for the back-propagated field $\phi(C)$:

$$\phi(C)=\mathrm{A}_G(|\mathbf{r}|,\varphi)X^{1/2}(p)\cos\varphi\ \exp\left[ik_0(\Phi(p)-\Phi_G(|\mathbf{r}|))\right]\left|\frac{\partial^2\Psi}{\partial\theta^2}\right|^{-1/2} \tag{71}$$

$$X^{1/2}(p)=\sqrt{\frac{pR_0}{p_s\sqrt{R_G^2-p^2}\sqrt{R_1^2-p^2}}\left|\frac{\partial\theta}{\partial p}\right|^{-1}} \tag{72}$$

$$\frac{\partial^2\Psi}{\partial\theta^2}=\frac{\frac{\partial\theta}{\partial p}-\frac{\partial(\theta-\theta_c)}{\partial p_b}}{\frac{\partial\theta}{\partial p}\frac{\partial(\theta-\theta_c)}{\partial p_b}} \tag{73}$$

The derivatives $\frac{\partial\theta}{\partial p},\frac{\partial(\theta-\theta_c)}{\partial p_b}$ can be found from the relationships (64), (68) as follows:

$$\frac{\partial\theta}{\partial p}=\frac{\partial\xi}{\partial p}-\frac{1}{\sqrt{R_G^2-p^2}}-\frac{1}{\sqrt{R_1^2-p^2}} \tag{74}$$

$$\frac{\partial(\theta-\theta_c)}{\partial p_b}=\frac{\partial\xi_m}{\partial p_b}+\frac{1}{\sqrt{n_m^2(R)R^2-p_b^2}}-\frac{1}{\sqrt{R_1^2-p_b^2}} \tag{75}$$

From (64)-(75) the following formula for $\chi=\left|\frac{\partial^2\Psi}{\partial\theta^2}\right|^{-1/2}$ can be derived:

$$\chi=\sqrt{\frac{\left|\left[\frac{\partial\xi_m}{\partial p_b}\sqrt{n_m^2(R)R^2-p^2}\sqrt{R_1^2-p^2}-|\mathbf{r}|'\right]\left(\frac{\partial\xi}{\partial p}\sqrt{R_G^2-p^2}\sqrt{R_1^2-p^2}-R_0'\right)\right|}{\left(R_L^2-p^2\right)\left|\left(\frac{\partial\xi_m}{\partial p_b}-\frac{\partial\xi}{\partial p}\right)\sqrt{n_m^2(R)R^2-p^2}\sqrt{R_G^2-p^2}+R_x\right|}} \tag{76}$$

$$\begin{aligned}&R_x=\sqrt{n_m^2(R)R^2-p^2}+\sqrt{R_G^2-p^2}\\&R_0'=\sqrt{R_G^2-p^2}+\sqrt{R_1^2-p^2}\approx R_0;\ |\mathbf{r}|'=\sqrt{R_1^2-p^2}-\sqrt{n_m^2(R)R^2-p^2}\approx|\mathbf{r}|\end{aligned} \tag{77}$$

Under condition:

$$n_m(R)R=p \tag{78}$$

the next relationship follows from eqns (72), (76), (77):

$$\chi X^{1/2} = \sqrt{\frac{R_0' \left|\mathbf{r}\right|' X \left| \left(\frac{\partial \xi}{\partial p} \frac{\sqrt{R_G^2 - p^2}\sqrt{R_1^2 - p^2}}{R_0} - 1 \right) \right|}{\sqrt{R_G^2 - p^2}\left(R_L^2 - p^2\right)}} = \sqrt{\frac{pR_0' \left|\mathbf{r}\right|' \left(R_1^2 - p^2\right)^{-1}}{p_s \sqrt{R_G^2 - p^2}}} \approx const \qquad (79)$$

where, p_s is the impact parameter corresponding to the straight line GL (Figure 2).) Factor $\chi X^{1/2}$ in (79) is independent of the refractive angles ξ and ξ_m. Therefore the amplitude variations are minimal at the geometric places in space determined by condition (78). According to [11] this corresponds to the position of a layer which can be estimated by finding the location of the minimum of the amplitude modulation of the 2-D back-propagating electromagnetic field. This property can be used as a main condition for locating layered structures in atmosphere and ionosphere. The accuracy of the location determination depends on: (i) the form of Green function used for the back-propagation; (ii) the structure and form of the (ionospheric) irregularities.

The simplest form of the Green function (58) has been used [10,11] to locate plasma layers in the E- and F- regions in the ionosphere. In this case $n_m(R) \equiv 1$, the back-propagated rays are straight lines, and condition (78) has the following form:

$$R = p \qquad (80)$$

From condition (80) the curve BB' in Figure 2 indicates the place, where the amplitude of the back-propagated field is constant. The curve BB' may be approximated by a straight line because the bending angle is small in the RO case. The inaccuracy in the determination of distance $T'L$ by back-propagation may be evaluated as the distance of the curve BB' to a new ray perigee T' $T'B \approx p'\xi/2$ (Figure 2). The proposed technique gets the length $T'L$ as the sum $TL + d$. The systematic inaccuracy of this technique is equal to the difference $T'L - TL - d$ which usually is smaller than that of the considered back-propagation method. For a more complex form of the Green function (59) the back-propagated rays are curved. If the Green function (59) corresponds to a real refractivity distribution in layered structures, then condition (78) gives an accurate location of the ray perigee T (Figure 2).

4.5. Locality principle and its importance for RO remote sensing

Locality principle allowed designing new analytic technique for locating the inclined layered structures (including sporadic E_s layers) in the ionosphere. The location of the ionospheric layers including their altitude, displacement from the RO ray perigee and slope relative to the horizontal direction can be determined using the introduced criterion that compares the refractive attenuations found from the RO amplitude and phase data. Depending on the sign of the refractive attenuations the displacement of a plasma layer from the RO ray perigee should be positive (in the direction to a GPS satellite and vise

versa). The magnitude of the displacement can be found from a ratio of the refractive attenuation's difference to the magnitude of the refractive attenuation from the RO phase data. The altitude and slope of a plasma layer can be found from the known value of its displacement.

Therefore the standard estimation of a layer's altitude as a height of RO ray perigee should be revised due to underestimation of the altitude of inclined plasma structures in the lower ionosphere.

The current radio-holographic back-propagation method implicitly uses the relationship between the eikonal acceleration and intensity variations of RO signals to locate irregularities in the ionosphere. The accuracy of this method depends on the form of the Green function used for the back-propagation. If the Green function corresponding to the propagation in the free space is used, then the inaccuracy of back-propagation method is proportional to the bending angle. The analytic technique is simpler and more precise than the previously published back-propagation method.

By use of the introduced criterion the RO method is capable to locate and determine the direction and magnitude of the gradient of electron density in the lower ionosphere. The gradient of the electron content indicates the direction of the different kinds of wave fronts in the ionosphere. In the particular case of the internal gravity waves (GW) the inclination of the wave vector to the vertical direction can be used to find the angular frequency and the parameters of GW.

The introduced criterion and technique extended the applicable domain of RO method to remote sense the waves in the lower ionosphere. This conclusion has a general importance for the planetary and terrestrial radio occultation experiments in a broad range of frequencies.

5. Bending angle: Seasonal changes

The RO method has important radio meteorological application. Previously the radio meteorological parameters (refractive angle, refractive attenuation, phase path excess, total absorption, and other) have been recalculated from the temperature, humidity and pressure delivered from the current meteorological observations. Nowadays the RO method directly measured the bending angle, refractive attenuation, phase path excess, total absorption, etc.) from the amplitude and phase delay of RO signal. Thus the RO radio meteorological observation are very important for estimation of condition for radio wave propagation, radio navigation, and radio climate in the near Earth space.

In this section the seasonal change of the bending angles as an important radio meteorological parameter will be considered.

Atmospheric refraction caused by gradients of the refractive index of air leads to a deviation of the direction of radio wave propagation from straight line connecting transmitter and receiver. Practical problems require to study variations of the bending angle, refractive

attenuation and other radio parameters as functions of the coordinates of transmitter and receiver. When the altitude of a radio link is low, changes in the vertical profiles of temperature, pressure and humidity introduce main contribution in the refraction effects. Meteorological parameters depend on the climate and weather in different geographical positions, which was the cause of origin of radio meteorology – a branch of radio science which used the weather information for analysis of the electromagnetic waves propagation conditions in radio communication and radar applications [38,57,58]. The vertical and horizontal distributions of the pressure, temperature, and humidity found from meteorological measurements are approximated by use of different models to find the altitude and spatial dependences of the refractive index, bending angle, refractive attenuation and absorption of radio waves. However the meteorological measurements are local, and relevant parameters are variable, which inevitably leads to discrepancy between the measured and calculated values of the bending angles.

The innovative RO method is a new important tool for direct measurements of the radio meteorological parameters and for investigation of radio climate of the Earth at different altitudes in the atmosphere with a global coverage. In contrast to previously used goniometric methods with a narrow antenna pattern or interferometers for measuring refraction effects and their variations in radio links, the RO method directly determines with high accuracy the bending angle from measurements of the Doppler frequency of radio wave. The measured bending angle does not depend on the wavelength, orbits of satellites, and characteristics of the transmitting and receiving devices. The measured bending angle is delivered with high accuracy without any assumptions concerning the structure of the atmosphere, and can be regarded as an independent quantitative radio meteorological parameter in different regions of the Earth. It is essential that the spatial and temporal distributions of refractive properties can be obtained over a long period of time, which will contain daily, seasonal, and long-term radio climatic changes in the atmosphere. This information can be applied for detailed analysis of radio wave propagation conditions along the Earth's surface.

The aim of this section is to establish the applicability of the bending angle as an indicator of the global state of the atmosphere. The annual and seasonal variations of the refractive parameters above Russia and some territories are analyzed and discussed.

5.1. Method of measurement

In determining the angle of refraction by the radio occultation method, the measured parameters of coherent radio waves with the frequencies $f_1 = 1575.42$ MHz and $f_2 = 1227.60$ MHz radiated by GPS satellites and received after transmission through the atmosphere were used. The radio waves were received by low earth orbit satellites FORMOSAT-3. A constellation of ~30 GPS satellites orbiting the Earth at a height of 20 000 km and of 6 low-earth-orbit satellites orbiting the Earth at a height of 800 km provided from 1400 to 1800 atmospheric soundings in various regions of the Earth. The measurements of the atmospheric component of the phase path increment and, respectively, of the Doppler shift

of the signal frequency, determined by the atmospheric refraction, were performed with a sampling frequency of 50 Hz. The mean time of sensing the atmosphere in the altitude 50 – 0 km interval was 90 s. Owing to refraction, the rate of changing of the height of the ray perigee decreases as the ray descends into denser layers of the atmosphere; therefore, the step of the measurement of the Doppler shift of the signal was ~50 m for stratosphere and ~5 m for the lower troposphere.

In analyzing the space–time variations of the bending angle, the results of 4252 occultation atmospheric soundings performed from June 2006 to July 2010 in the region of European Russia with coordinates of 50°N to 60°N and 30°E to 40°E were used. The extent of this region is 1100 km along the meridian and ~600 km along the latitude circle. In this region, three to seven measurement sessions were conducted every day.

The method for determining the bending angle $\xi(h)$ as a function of the minimum ray path height is based on the relation between the atmospheric component of Doppler frequency shift Δf_a and $\xi(h)$. This relation is most simple for the occultation sensing, when one of the satellites is at a large distance from the ray path perigee. In this case $\Delta f_a \approx \lambda^{-1} V_1 \xi(h)$, where λ is the wavelength, V_1 is the projection of the vector of the satellite velocity in the occultation plane on the perpendicular to the straight line connecting the satellites. The accuracy of determining the angle of refraction depends on the error of the frequency shift measurement, which is affected by the errors of measuring the atmospheric phase path increment, coordinates, velocities of the navigation and low earth orbit satellites, and also by the influence of the ionosphere and multipath propagation. The contribution of these errors is analyzed in detail in study [59]. This contribution can be minimized by improving the receiving equipment installed on the low earth orbit satellite and the procedures for measuring and processing the raw data. At present, the instrumental error of the bending angle measurements is no more than $5 \cdot 10^{-7}$ rad.

The sources of systematic error are related to the effect of the ionosphere and multipath propagation. The influence of the ionosphere is eliminated using two frequency ionospheric correction [53]. However, the ionospheric correction cannot completely remove the bending angle fluctuations caused by small scale electron concentration irregularities. In sensing the upper stratosphere, the bending angle errors caused by this factor can be as high as $3 \cdot 10^{-6}$ rad, but they rapidly decrease as the height decreases [55]. Below 30 km, this error component can be ignored. Of greater importance to meteorological applications are the refractive angle errors caused by multipath in sensing the lower troposphere. To solve this problem, several radio-holography methods for processing occultation data have been developed. The number of publications on this subject is very large, the descriptions of these methods and references to the original publications are given in [38,60].

The refractive angle is determined from the measurements of the signal frequency, a quantity that can be measured with a maximum accuracy. The results of the analysis made in [61] show that, in the middle latitude atmosphere, at heights of 5 to 30 km, the discrepancy between the measured and calculated (with the use of various models of the

atmosphere) bending angles does not exceed ±1%. The height profile of the bending angle may contain inaccuracies related to the errors in height measurements. At the initial stage of data processing, the dependence of the refractive angle $\xi(p)$ on the impact parameter $p = (\rho_e + h)n(\rho_e + h)$ is determined where ρ_e is the Earth's radius. The height of the atmospheric layer is determined as the height above the surface of the geoid described by reference ellipsoid WGS84 (World Geodetic System 1984). The error of the height evaluation in our data does not exceed ±100 m. It is necessary to study the variability of the refractive angle height profiles at different time periods and in various regions of the Earth. As an example such an analysis is performed using a vast region of Russia.

5.2. Mean bending angle vertical profile

In analyzing space–time refraction variations, one should eliminate the influence of the regular component. To this end, a model of the bending angle vertical profile $\xi(h)$ derived, e.g., from long term observations is required. It is clear that regional models of $\xi(h)$ are in better agreement with the measurement results than the global model. The variability of the parameters of these models for different regions is of interest for radio-meteorology. As an example, the vertical profiles $\xi(h)$ for the middle latitudes of Russia are described in this section. The mean vertical profile of $\xi(h)$ and ranges of variations of the refractive angle at different heights were obtained by averaging the data of 8711 measurement sessions performed during a four year period. In addition to the data obtained in the region with coordinates of 50°N to 60°N and 30°E to 40°E, the results of 4459 atmospheric soundings performed in the same latitude belt of 50°N to 60°N but at a longitude of 160°E to 170°E were used. A second region includes Kamchatka's eastern coast and the adjacent water area of the Bering Sea and is characterized by marine climate. The use of the measurement data obtained in the two regions allowed deriving analytical dependence $\xi(h)$ suitable for analyzing the space–time variations of the refractive angle observed in the regions that are in different climatic conditions. The performed analysis showed that, in the altitude range from 0 to 50 km, the mean vertical profile of the refractive angle $\xi_a(h)$ is described by

$$\xi_a(h) = \exp\left(a + bh + ch^2 + d_1^3\right) \tag{81}$$

If the bending angle is expressed in milliradians and the height is expressed in kilometers, the coefficients in the exponent (81) have the values given in Table 1.

h, km	a	b km^{-1}	c km^{-2}	d_1 km^{-3}
≤ 12.4	3.226	–0.154	3.765×10^{-3}	-1.487×10^{-3}
≥ 12.4	3.611	–0.166	4.128×10^{-4}	-6.374×10^{-6}

Table 1. Coefficients in equation (1)

The height profiles of the refractive angles measured in the two regions and calculated with model (1) are compared in Table 2. Root mean square values of σ_m significantly exceed the

measurement errors and characterize essential refraction variations caused by the difference of the meteorological conditions.

h, km	ξ_m, mrad	σ_m, mrad	ξ_a, mrad	$\xi_m - \xi_a$, mrad
0.2	23.96	2.19	24.41	–0.45
0.4	23.57	2.25	23.68	-0.11
0.6	23.03	2.23	22.98	0.06
0.8	22.50	2.19	22.30	0.20
1	21.95	2.15	21.65	0.29
2	19.94	1.91	18.75	0.19
3	16.16	1.43	16.32	-0.16
4	13.99	0.98	14.28	-0.29
5	12.26	0.64	12.25	-0.29
6	10.88	0.45	11.06	-0.18
7	9.76	0.38	9.76	-0.01
8	8.82	0.35	8.63	0.18
9	7.99	0.32	7.64	0.35
10	7.17	0.34	6.75	0.41
12	5.36	0.42	5.25	0.11
14	3.83	0.21	3.87	-0.04
16	2.81	0.15	2.82	-0.01
18	2.07	0.11	2.06	0.01
20	1.51	0.08	1.50	0.01
25	0.69	0.04	0.68	0.002
30	0.31	0.02	0.31	-0.003

Note: h is the height of the ray perigee relative to the Earth's surface, ξ_m, ξ_a are the bending angles determined by averaging from the measured data and calculated with model (1), respectively, σ_m is the rms value of the bending angle for the four year period.

Table 2. Comparison of the averaged height profiles and variations of the refractive angle

Of interest is the distribution of these variations. The refractive angle disturbances at the corresponding heights are distributed, with respect to the mean value of ξ_m in accordance with a near normal law. In 90% of the measurements, for heights h = 0.2, 1, 4, and 8 km, the mean refractive angles are 23.88 ± 3.63, 22.12 ± 3.72, 13.98 ± 1.71, and 8.76 ± 0.51 mrad, respectively. It follows from Table 2 that the largest absolute and relative variations σ_m, σ_m / ξ_m of the refractive angle are observed in the troposphere at altitudes below 8 km. These variations are due to weather changes in the regions being sounded. In the stratosphere above 14 km, relative refractive angle variations σ_m / ξ_m are approximately half the same one in the troposphere. Model (81) of the refractive angle altitude profile is in good agreement with the experimental data, since its deviation from the mean bending angle, ξ_m, is several times smaller than the observed rms variations σ_m. At heights above 14 km, the

deviation of the experimental data from the model data is no more than 1%. Note that analytical model (1) with the coefficients listed in Table 1 does not describe the individual features of the refraction that are, e.g., related to the influence of the tropopause. This factor is responsible for the marked difference between ξ_m and ξ_a over the altitude interval from 9 to 12 km, heights that are typical for the tropopause in the midlatitudes. It should also be noted that this model is not intended for deriving meteorological parameters, e.g., a temperature–height profile. The model describes a significant decrease in refraction over the height interval from 0 to 30 km. The model can be used in detecting small regional and seasonal variations of the vertical profile.

5.3. Seasonal and diurnal bending angle variations

The bending angle rapidly decreases from ~24 mrad to ~0.3 mrad as the ray perigee height h increases from h = 0.2 km to h = 30 km. In analyzing small bending angle disturbances, caused by various factors, it is necessary to eliminate the component related to a rapid decrease in the atmospheric density occurring with an increase in height. To this end, it is possible to use obtained approximation of mean height profile of the bending angle ξ_a (81) and consider the refractive angle disturbances observed in individual measurement sessions in reference to this approximation. The most significant refractive angle disturbances are observed in the troposphere and lower stratosphere. Therefore, in analyzing the disturbances in angle ξ, we will restrict our consideration to a height interval of 0 to 14 km and compare the observational results obtained in summer and in winter.

As an illustration of slow disturbances in the height profile of the bending angle, let us consider the vertical profiles of the deviations of the refractive angles, observed in individual measurement sessions, from the values calculated with model (81), i.e., $\Delta\xi(h) = \xi - \xi_a$). Profile $\Delta\xi(h)$ allows detecting influence of regular layered structures of various nature on the refraction.

Shown in Figure 8 are four profiles $\Delta\xi(h)$ obtained in morning, in January 2007. The conditions for measurements are determined by the day of the year (DOY) counted from January 1, by the Universal Time Coordinated (UTC) expressed in hours and minutes, and by the geographic latitude and longitude of the region (Table 3). The time and the coordinates of the region are usually given for the moment when the straight satellite to satellite line touches the Earth's surface. This moment corresponds to the ray perigee height h ~ 13 km. The local time (LT) in the region being sounded is, on the average, three hours later than the UTC. The winter night is characterized by a stationary state of the troposphere with layered structures and pronounced maximums of $\Delta\xi(h)$ at heights of 1.5–2.7 km and 3.5–4 km, which correspond to significant vertical gradients of refractivity. The maximum values of $\Delta\xi(h)$ are as high as 4 mrad, and the thickness of the layers is 0.7 to 1.5 km. Stronger disturbances were observed in July 2010. In summer daytime, the deviations of the refractive angle from the mean values are 4–10 mrad at heights of 0.7 to 5 km. It seems likely that this phenomenon is due to a higher content of water vapor and significant variations in

the vertical distribution of water vapor in summer as compared to winter. For the height interval of 9 to 14 km, depending on the season and time of day, smooth refractive angle deviations from mean values $\Delta\xi(h)$, caused by the temperature inversion in the tropopause, are recorded. Unlike the refractive angle disturbances in the lower troposphere, which are, as a rule, related to the variations in humidity, the temperature inversion in the tropopause results in an insignificant increase of angle ξ in a range of 0.6 to 1.3 mrad. With a narrow tropopause, the position of the local maximum of $\Delta\xi(h)$ is close to the height of the minimum temperature, which is determined from the occultation sounding data and meteorological sounder measurements.

Curves in Figure 4	Date January 2007	UTC, h, min	N, deg	E, degr.	Curves in Figure 4	Date January 2007	UTC, h, min	N, deg	E, deg
1	01	04:34	57.34	39.9	5	10	04:17	58.29	41.71
2	01	04:44	53.99	39.31	6	20	16:19	56.51	42.56
3	06	05:10	54.03	34.66	7	19	06:26	53.41	35.62
4	10	04:05	58.03	33.55	8	20	06:41	57.54	41.76

Table 3. Coordinates and time of experiments

In addition to slow (seasonal and diurnal) variations in the refractive angle, significant rapid fluctuations caused by atmospheric irregularities are observed. Using the results of 200 measurement sessions, the fluctuations of the bending angle observed in winter and in summer without separating them in time of day were analyzed. It is necessary to eliminate the regular and slow variations in order to estimate the rapid fluctuations. To this end, a filtering procedure was used that involves subtraction of function $\xi_S(h)$ obtained by smoothing the refractive angle in the sliding window $\Delta h = 2$ km.

Changes in the conditions of refraction in regions with different climates and on different time scales will have both individual and general laws. To detect these patterns let us look at the changes of refraction in a homogeneous area of the climatic conditions at different time intervals and analyze the seasonal and annual changes. To reduce the influence of spatial factors let us to limit the area in which the seasonal variations in the angle of refraction are investigated, and to select the cell size of approximately 400x400 km^2, extending in latitude from 54.0 N to 58.0 N and longitude from 35.0 E to 41.0 E. The center of this area is located in the vicinity of Moscow. In the period from January 1, 2007 and November 30, 2009 in this area was carried out 1232 RO soundings of the atmosphere. In each month of the year from 25 to 29 soundings at different times of day were held. Let us consider the seasonal changes of the bending angle at two altitudes: in the middle stratosphere at 15 km, and in the upper troposphere at 9 km (Figure 8). Note that the most accurate radio occultation measurements in the stratosphere and upper troposphere have been provided at these altitudes. At the altitude 17 km in the middle stratosphere, there is a positive trend, i.e. strengthening of refraction with time. This increase is nearly equal to 0.07. mrad during four years. In

contrast to the stratospheric region in the upper troposphere at an altitude of 9 km in the period under review there was a negative trend in refraction, whose value is amounted to 0.11 mrad. When reducing the height, this trend is weakening and at the altitude 4 km the long-term trend of refraction is practically not observed.

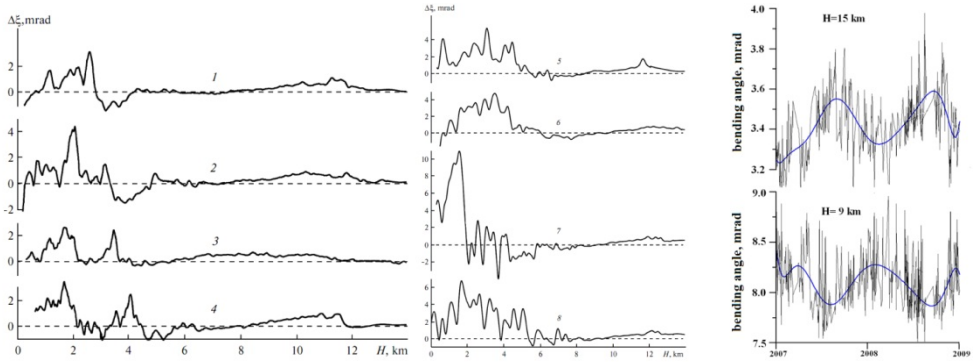

Figure 8. Left panel. Examples of the refractive angle variations obtained in January 2007. Middle panel. Examples of the refractive angle variations obtained in July 2010. Right panel. Annual changes of the bending angle at the 9 km and 15 km altitudes from FORMOSAT-3 RO data in Moscow region.

The future task is to investigate the trends as functions of time and geographical position in different climatic zones for longer periods. However it is clear is that the angle of refraction is a sensitive indicator of the state of the troposphere – stratosphere system. Seasonal changes in the refractive properties observed in the stratosphere and the troposphere are evident, but they manifest themselves in different ways. In the stratosphere, there are quasi-harmonic changes with a period of 12 ± 0.5 months and the amplitude of about 0.12 mrad relative to the average trend. Maximum values of the bending angle occur in late July - early August, and the minimal during February - March. Seasonal changes in the upper troposphere also contain a component with a period of 12 ± 0.5 months, but they are opposite to the phase variations in the stratosphere. Their amplitude is in average 0.23 mrad. The maximum refraction occurs in March near the vernal equinox, and the minimum - in August. The influence of a weak quasi-monochromatic component is seen in the middle troposphere at an altitude of 4 km in the bending angle variations. Maximum values of the bending angle is ~ 15 mrad are observed, usually in late summer - early autumn, and in the rest of the year they are 3-5 mrad. This behavior corresponds to refraction in the middle and lower troposphere due to weather changes, which essentially smoothes the effect of changing seasons of the year.

6. Conclusions

The fundamental principle of local interaction of radio waves with a spherically symmetric medium is formulated and introduced in the RO method of remote sensing of the atmosphere and ionosphere of the Earth and planets.

In accordance with this principle, the main contribution to variations of the amplitude and phase of radio waves propagating through a medium makes a neighborhood of a tangential point where gradient of the refractive index is perpendicular to the radio ray.

A necessary and sufficient condition (a criterion) is established to detect from analysis of RO data the displacement of the tangential point from the radio ray perigee.

This criterion is applied to the identification and location of layers in the atmosphere and ionosphere by use of GPS RO data. RO data from the CHAllenge Minisatellite Payload (CHAMP) are used to validate the criterion introduced when significant variations of the amplitude and phase of the RO signals are observed at RO ray perigee altitudes below 80 km.

The new criterion provides an improved estimation of the altitude and location of the ionospheric plasma layers compared with the back-propagation radio-holographic method previously used.

The detected criterion opens a new avenue in terms of measuring the altitude and slope of the atmospheric and ionospheric layers. This is important for the location determination of the wind shear and the direction of internal wave propagation in the lower ionosphere, and possibly in the atmosphere.

The locality principle makes it possible to convert the eikonal acceleration (or the time derivative of the Doppler shift) into refractive attenuation. This is important for estimation of the total absorption of radio waves on the satellite-to-satellite transionospheric communication paths. This dependence is also important for measuring the water vapor content and atmospheric gas minorities in the future radio-occultation missions in view of the possibility to remove the refractive attenuation effect from the amplitude data. The advantages of the proposed method were tested by analysis of the CHAMP satellite radio-occultation data.

The obtained results indicate that measurements of the total absorption on radio occultation paths can potentially be used for monitoring of the atmospheric-oxygen content provided that the transmitter and receiver gain calibration is substantially improved. It follows from the above analysis that the comparison of the refractive attenuations retrieved from the amplitude and phase variations of a radio-occultation signal is necessary for the detection of layered structures in the atmosphere.

The total absorption, refractive attenuation, bending angle, bending angle, and index of refraction are important radio meteorological parameters which can be measured directly with a high accuracy by the radio occultation method. The prolonged radio occultation data base is very important for determination of the radio climate changes at different altitudes in the atmosphere with a global coverage.

Author details

Alexey Pavelyev, Alexander Pavelyev, Stanislav Matyugov and Oleg Yakovlev
FIRE RAS, Fryazino, Russia

Yuei-An Liou
CSRSR, NCU, Taiwan

Kefei Zhang
RMIT University School of Mathemathical & Geospatial Sciences, Melbourne, Australia

Jens Wickert
GeoForschungsZentrum Potsdam (GFZ-Potsdam), Telegrafenberg, Potsdam, Germany

Acknowledgement

This work was supported in part by Russian Fund of Basic Research (grant No. 10-02-01015-a), Program of Presidium RAS No. 22, Program PSD- IY.13 of the Branch of Physical Sciences of the Russian Academy of Sciences, by Grants of the National Science Council of Taiwan NSC 101-2111-M-008-018; 101-2221-E-008-0, by Australian Research Council Project ARC-LP0883288 of the Department of Industry, Innovation, Science, and Research of Australia International Science Linkage under Project DIISR/ISL-CG130127, and by the Australia Space Research Program Project endorsed to research consortiums led by the Royal Melbourne Institute of Technology University. The authors are grateful to the GeoForschungsZentrum (Potsdam, Germany) for the data obtained during the CHAMP satellite mission.

7. References

[1] Yakovlev O. Space Radio Science. London: Taylor and Francis; 2003.
[2] Gurvich A, Krasilnikova T. Application of the navigational satellites for radio occultation of the Earth's atmosphere. Cosmic Res.1987 6: 89-95.
[3] Melbourne W. Radio Occultations Using Earth Satellites: A Wave Theory Treatment, Jet Propulsion Laboratory, California Institute of Technology, Boulder, 2004.
[4] Liou Y, Pavelyev A. Simultaneous observations of radio wave phase and intensity variations for locating the plasma layers in the ionosphere. Geophys. Res. Lett. 2006; 33: L23102.
[5] Pavelyev A, Liou Y, Wickert J, et al. Effects of the ionosphere and solar activity on radio occultation signals: Application to CHAllenging Minisatellite Payload satellite observations. J. Geophys. Res. 2007; 112: A06326, doi: 10.1029/2006JA011625.
[6] Liou Y, Pavelyev A, Liu S, et al. FORMOSAT-3/COSMIC GPS Radio Occultation Mission: Preliminary Results. IEEE Trans. Geosci. Remote Sensing 2007; 45: 3813-3823.
[7] Pavelyev A, Wickert J, Liou Y. Localization of plasma layers in the ionosphere based on observing variations in the phase and amplitude of radio waves along the satellite-to-satellite path. Radiophys. Quantum Electron 2008; 51(1): 1-7
[8] Pavelyev A, Liou Y, Wickert J, et al. Location of layered structures in the ionosphere and atmosphere by use of GPS occultation data. Adv. Space Res. 2008; 42: 224-228.
[9] Sokolovskiy S. Inversion of radio occultation amplitude data. Radio Sci. 2000; 35: 97-105.

[10] Gorbunov M, Gurvich A, Shmakov A. Back-propagation and radioholographic methods for investigation of sporadic ionospheric E-layers from Microlab-1 data. Int. J. Remote Sensing 2002; 23: 675-682.

[11] Sokolovskiy S, Schreiner W, Rocken C, Hunt D. Detection of high-altitude ionospheric irregularities with GPS/MET. Geophys. Res. Lett. 2002; 29: 1033-1037.

[12] Pavelyev A, Zakharov A, Kucheryavenkov A, et al. The features of propagation of radio wave reflected from terrestrial surface at small elevation angles on radio telecommunication link low orbital satellite-GEO. J. Commun. Tech. Electron 1997; 42: 45-51.

[13] Pavelyev A, Volkov A, Zakharov A, et al. Bistatic radar as a tool for the Earth's observation using small satellites. Acta Astronautica 1996; 39: 721-730.

[14] Kirchengast G, Hoeg P in: Steiner A, Kirchengast G, Foelsche U Eds. Occultations for Probing Atmosphere and Climate, Springer, New York 2004; 201-212.

[15] Gorbunov M, Kirchengast G. Processing X/K Band Radio Occultation Data in Presence of Turbulence. Radio Sci. 2005; 40: RS6001.

[16] Lohman M, Jensen A, Benzon H, Nielsen A. Radio Occultation Retrieval of Atmospheric Absorption based on FSI. Report 03-20, Danish Meteorological Institute: Copenhagen; 2003.

[17] Jensen A, Lohmann M, Nielsen A,. Benzon H. Full Spectrum Inversion of Radio Occultation Signals. Radio Sci.2003; 39: 1040-1052.

[18] Yakovlev O, Yuakubov V, Uruadov V, Pavelyev A. Radio waves propagation. Moscow Lenand Ed; 2009.

[19] Kravtsov Yu., Orlov Y. Geometrical Optics of Inhomogeneous Media. Springer: Berlin; 1990.

[20] Pavelyev A, Kucheryavenkov A. On a possibility of investigation of the Earth's atmosphere by radio occultation method. J. Commun. Tech. Electron. 1978; 7: 1345-1353.

[21] Kislyakov A, Stankevich K. Absorption of radio waves in the atmosphere. Radiophys. Quantum Electron. 1967; 10: 1244-1268.

[22] Yakovlev O, Matyugov S, Vilkov I. Attenuation and scintillation of radio waves in the atmosphere from data of radio occultation experiments in the satellite-to-satellite link. Radio Sci. 1995; 30: 591-599.

[23] Rius A, Ruffini G, Romeo A. Analysis of ionospheric electron density distribution from GPS/MET occultations. IEEE Trans. Geosci. Remote Sens. 1998; 36(2): 383–394.

[24] Hajj G, Romans L. Ionospheric electron density profiles obtained with the Global Positioning System: Results from GPS/MET experiment. Radio Sci. 1998; 33(1) 175-190.

[25] Igarashi K, Pavelyev A, Hocke K, Pavelyev D, Wickert J. Observation of wave structures in the upper atmosphere by means of radio holographic analysis of the radio occultation data. Advances in Space Research 2001; 27: 1321-1326.

[26] Wickert J, Reigber C, Beyerle G, Konig R, Marquardt C, Schmidt T, Grunwaldt L, Galas R, Meehan T,. Melbourne W, Hocke K. Atmosphere sounding by GPS radio occultation: First results from CHAMP. Geophys. Res. Lett. 2001; 28(9): 3263–3266.

[27] Wickert J, Pavelyev A, Liou Y, Schmidt T, Reigber C, Igarashi K, Pavelyev A, Matyugov S. Amplitude scintillations in GPS signals as a possible indicator of ionospheric structures. Geophys. Res. Lett. 2004; 31(15): L24801, 1-4.

[28] Wu D, Ao C, Hajj G, Juarez de la Torre, J. Mannucci A. Sporadic E morphology from GPS-CHAMP radio occultation. J. Geophys. Res. 2005; 110: A01306, doi:10.1029/2004JA010701.

[29] Pavelyev A, Liou Y, Huang C, Reigber C, Wickert J, Igarashi K, Hocke K. Radio holographic method for the study of the ionosphere, atmosphere and terrestrial surface using GPS occultation signals. GPS Solut., 2002; 6: 101-108.

[30] Pavelyev A, Liou Y, Wickert J. Diffractive vector and scalar integrals for bistatic radio-holographic remote sensing. Radio Sci. 2004; 39(4): RS4011, 1-16, doi:10.1029/2003RS002935.

[31] Pavelyev A, Liou Y, Wickert J, Gavrik A, Lee C. Eikonal acceleration technique for studying of the Earth and planetary atmospheres by radio occultation method. Geophys. Res. Lett. 2009; 36. doi:10.1029/2009GL040979, L21807, 1-5.

[32] Pavelyev A, Zhang K, Wang C, Kuleshov Y, Liou Y, Wickert J. Identification of Inclined Ionospheric Layers Using Analysis of GPS Occultation Data. IEEE Trans. Geosci. Rem. Sens. 2011; 49(6): part 2, 2374-2384. doi:10.1109/TGRS.2010.2091138.

[33] Liou Y,. Pavelyev A, Huang C, Igarashi K, Hocke K. Simultaneous observation of the vertical gradients of refractivity in the atmosphere and electron density in the lower ionosphere by radio occultation amplitude method. Geophys. Res. Lett. 2002; 29(19), 43-1-43-4. doi:10.1029/2002GL015155.

[34] Liou Y, Pavelyev A, Huang C, Igarashi K, Hocke K, Yan S. Analytic method for observation of the GW using RO data. Geophys. Res. Lett. 2003; 30(20): ASC 1-1 – 1-5., doi:10.1029/2003GL017818.

[35] Liou Y, Pavelyev A, Pavelyev A, Wickert J, Schmidt T. Analysis of atmospheric and ionospheric structures using the GPS/MET and CHAMP radio occultation data base: A methodological review. GPS Solut. 2005; 9 (2): 122–143.

[36] Pavelyev A, Liou Y, Zhang K et al. Identification and localization of layers in the ionosphere using the eikonal and amplitude of radio occultation signals Atmos. Meas. Tech., 2012; 5(1): 1–16, doi:10.5194/amt-5-1-2012.

[37] Pavelyev A, Zhang K, Wang C et al. Analytical method for determining the location of ionospheric and atmospheric layers from radio occultation data Radiophys. Quantum Electron 2012; 55(3): 168-175.

[38] Liou Y, Pavelyev A, Matyugov S, Yakovlev O, Wickert J. 2010 Radio Occultation Method for Remote Sensing of the Atmosphere and Ionosphere. Edited by Liou Y. INTECH Published by In-The Olajnica 19/2, 32000 Vukovar, Croatia, 170, 45, ISBN 978-953-7619-60-2.

[39] Arras C, Wickert J, Jacobi C, Heise S, Beyerle G. Schmidt T. A global climatology of ionospheric irregularities derived from GPS radio occultation. Geophys. Res. Lett. 2008; 35, L14809, doi: 10.1029/2008GL034158.

[40] Arras C, Jacobi C, Wickert J. Semidiurnal tidal signature in sporadic E occurrence rates derived from GPS radio occultation measurements at higher midlatitudes. Ann. Geophys., 2009; 27: 2555–2563.

[41] Arras C, Jacobi C, Wickert J, Heise S, Schmidt T. (2010), Sporadic E signatures revealed from multi-satellite radio occultation measurements. Adv. Radio Sci. 2010; 8: 225–230. doi:10.5194/ars-8-225-2010.

[42] Jakowski N, Leitinger R, Angling M. (2004), Radio occultation techniques for probing the ionosphere. Ann. Geophys. 2004; supplement to 47(2/3): 1049-1066.

[43] Kunitsyn V, Tereshchenko E. Ionospheric Tomography. Springer-Verlag: Berlin: 2003.

[44] Kelley M, Wong V, Hajj G, Mannucci A. On measuring the off-equatorial conductivity before and during convective ionospheric storms. Geophys. Res. Lett. 2004; 31: L17805, doi:10.1029/2004GL020423.

[45] Kelley M, Heelis A. The Earth's ionosphere: plasma physics and electrodynamics. Elsevier Science.2009; 96: 556, International geophysics Second Edition Cornell University Engineering School of Electrical Engineering Academic Press, ISBN 10: 0120884259/0-12-088425-9, ISBN 13: 9780120884254

[46] Pavelyev A, Liou Y, Wickert J, Zhang K, Wang C, Kuleshov Y. Analytical model of electromagnetic waves propagation and location of inclined plasma layers using occultation data. Prog. Electromagn. Res. 2010; 106: 177-202, doi: 10.2528/PIER10042707.

[47] Pavelyev A, Liou Y, Wickert J, Schmidt T, Pavelyev A, Matyugov S. Phase acceleration: a new important parameter in GPS occultation technology. GPS Solut. 2010; 14(1): 3-14. doi:10.1007/s10291-009-0128-1.

[48] Whitehead J. The formation of the sporadic-E layer in the temperate zones. J. Atmos. Terr. Phys. 1961; 20 49–58.

[49] Plane J. (2003), Atmospheric Chemistry of Meteoric Metals. Chem. Rev. 2003; 103. 4963–4984.

[50] Pavelyev A, Tsuda T, Igarashi K, Liou Y, Hocke K. Wave structures in the electron density profile in the ionospheric D and E-layers observed by radio holography analysis of the GPS/MET radio occultation data. J. Atmos. Solar-Terr. Phys. 2003; 65(1): 59-70.

[51] Haldoupis C, Pancheva D, Singer W. Meek C, Mac-Dougall J. An explanation for the seasonal dependence of midlatitude sporadic E layers. J. Geophys. Res. 2007; 112: A06315, doi:10.1029/2007JA012322.

[52] Melbourne W, Davis E, Duncan C, Hajj G, Hardy K, Kursinski E, Meehan T, Young L, Yunck T. The Application of Spaceborne GPS to Atmospheric Limb Sounding and Global Change Monitoring. Jet Propul. Lab., Pasadena, Calif. 1994; 94-18: 147.

[53] Vorob'ev V, Gurvich A, Kan V, Sokolovskiy S, Fedorova O, Shmakov A. (1997), The structure of the ionosphere from the GPS-"Microlab-1" radio occultation data: Preliminary results. Cosmic Research 4, 74-83. (In Russian)

[54] Gubenko V, Pavelyev A, Andreev V. Identification of wave origin of temperature fluctuations and determination of the intrinsic frequency of internal gravity waves in the Earth's stratosphere derived from radio occultation data. J. Geophys. Res. 2008; 113: D08109, doi:10.1029/2007JD008920.

[55] Hocke K. Inversion of GPS meteorology data, Ann. Geophys. 1997;15. 143-152.

[56] Gorbunov M, Sokolovskiy S, Bengtson L. Advanced algorithms of inversion of GPS/MET satellite data and their application to reconstruction of temperature and humidity Tech. Rep Report No. 211. Max Planck Institute for Meteorology. Hamburg. 1996.

[57] Bean B, Dutton E. Radio Meteorology. Central Bureau of Standards. Boulder. Colorado. 435 p., 1966.

[58] Kolosov M, Shabel'nikov A. Refraction of Electromagnetic Waves in the Atmosphere of the Earth, Venus and Mars (Sovetskoe Radio, Moscow, 1976) [in Russian].

[59] Kursinski E, Hajj G, Hardy K, Linfield R, Hardy K. Observing Earth's atmosphere with radio occultation measurements using the Global Positioning System. J. Geophys. Res. 1997; 102 (D19), 23429.

[60] Yakovlev O, Pavelyev A, Matyugov S. Satellite Monitoring of the Earth: Radio Occultation Monitoring of the Atmosphere and Ionosphere (Librokom, Moscow, 2010) [in Russian].

[61] Loescher A, Lauritsen K, Sørensen M. The GRAS SAF Radio Occultation Processing Inter comparison Project ROPIC New Horizons in Occultation Research (Springer Verlag, Heidelberg, 2009), pp. 49–62.